Analysing riverbank and plastic spectra across remote sensing sensors to examine plastic detectability

by
Milou Maathuis

A Master's Thesis
Thesis report - GIRS-2025-18
Geo-information Science and Remote Sensing
Wageningen University & Research
11th of June 2025

Analysing riverbank and plastic spectra across remote sensing sensors to examine plastic detectability

Milou Maathuis
Student number 1049299

Supervisors:

Marc Rußwurm
Tim van Emmerik

A thesis submitted in partial fulfilment of the degree of Master of Science

at Wageningen University and Research,

The Netherlands.

11th of June 2025

Thesis code number: GRS-80436
Thesis Report: GIRS-2025 -18
Wageningen University and Research
Laboratory of Geo-Information Science and Remote Sensing

Acknowledgements

I would like to express my appreciation to my supervisors, who provided guidance and expertise throughout the extensive and educational process of completing my master's thesis. I have learned a lot from both of you! A special thanks to Mathias Bochow from GFZ Potsdam, who supplied the majority of the plastic material and provided expertise in designing the field experiment. I am also very grateful for Berry Onderstal and Nick Wallerstein, who not only helped me with supplying measuring devices and other materials for my fieldwork, but also helped to think along with the practicalities and logistics. I am very grateful to my family and friends who helped with my fieldwork and with the collection of the PET bottles, and who also provided emotional support that has kept my motivation high throughout the thesis. I would like to acknowledge the help with the MAIA S2 camera by Ámbar Pérez-García and the help with the handheld spectroradiometer by Harm Bartholomeus. I would like to thank Nandika Tsendbazar and Giel Hagenbeek for their feedback on my research proposal.

Table of Contents

Abstract

Plastic poses a special threat to ecosystems and biodiversity because of its abundance in nature and longevity. Plastic monitoring in riverine environments is important as rivers are major transportation and storage systems of plastics. Remote sensing detection methods offer an opportunity to upscale riverine plastic monitoring. However, there is a clear need for more research on this topic. In this study, remote sensing detection of plastics on riverbanks is investigated by means of a field experiment in which two artificial plastic targets were placed on the riverbanks of the Nederrijn. One target consisted of white polyester sheets to increase the chances of a clear signal. The other target consisted of PET bottles, which are a more common form of plastic pollution. Data was collected with a variety of remote sensing sensors, covering a range of spatial, spectral, and temporal resolutions: The ASD Handheld 2 Spectroradiometer, the MAIA S2 multispectral camera, Sentinel-2 satellites, PlanetScope SuperDove satellites, and the EnMAP satellite. The collected reflectance spectra were analysed, and a spectral index analysis was done, combined with Naive Bayes classification. Sentinel-2 imagery proved to be useful for polyester detection, as the targets of 1x30 m, 2x30 m, and 3x30 m could be detected. The analysis showed the importance of high-resolution images to detect PET bottles. In addition, high correlations were found between polyester target size and several spectral indices, with the highest correlation coefficient being -0.93 for the Normalised Difference Aquatic Vegetation Index (NDAVI). This paper serves as a proof of concept to show that plastic detection in riverbank environments by using satellite and camera imagery is feasible and should be investigated further.

1. Introduction

Plastic poses a special threat to ecosystems and biodiversity because of its abundance in nature and longevity (Gall & Thompson, 2015; Gallitelli et al., 2020; Rillig, 2012; Strungaru et al., 2019). Animals ingest plastics or can get entangled in large pieces of plastic (Gall & Thompson, 2015). Humans are exposed to plastics as well, which can have severe health consequences (Yee et al., 2021). Plastics pose a risk not only to human health but also to human livelihood. For example, macroplastics can clog drainage systems which increases flooding risks, and plastic accumulations on riverbanks can have negative consequences for tourism (van Emmerik & Schwarz, 2020).

Plastic monitoring in river systems is needed to understand plastic transport and storage, and to eventually reduce plastic pollution (van Emmerik et al., 2023a). Rivers form main transportation and storage systems of plastics. Transportation behaviour of plastics is influenced by plastic properties that vary over plastic type (Tasseron et al., 2021). For example, low-density plastic floats on river water, while high-density plastics are submerged. Plastic size influences transportation as well. Macroplastics (> 25 mm) can fragment into smaller pieces and ultimately into microplastics (1 - 5 mm) (Lee et al., 2013). Microplastics undergo more complex transportation routes and are more easily taken up by organisms than macroplastics (Li et al., 2020). Rivers carry plastics towards the oceans, but on a global scale only a very small part of the total plastic pollution is estimated to end up in the ocean (Meijer et al., 2021). Large amounts of plastics can remain in river systems for a long time, which can be explained by the short travel distances in rivers due to entrapment in vegetation, and continual deposition on floodplains and riverbanks (Gallitelli et al., 2024; Hauk et al., 2023; Ledieu et al., 2022; Lotcheris et al., 2024; Schreyers et al., 2021; Tramoy et al., 2020; van Emmerik et al., 2022; van Emmerik et al., 2023b). Tramoy et al. (2020) found evidence that rivers can retain plastics for decades through bank deposition.

Remote sensing detection methods offer an opportunity to upscale riverine plastic monitoring, allow for reaching remote places, and allow for plastic detection beyond the RGB spectrum. Plastic pollution on riverbanks is often monitored by visual counting and collection, which is a slow and labour-intensive process (Maharjan et al., 2022; L. J. Schreyers et al., 2025; Vriend et al., 2020). The upscaling of riverine plastic monitoring has already been done through citizen science, in which citizens help to monitor plastics. However, there are difficulties in incentivizing citizens to participate, and not all river areas where plastics accumulate are easily accessible to humans (Fritz et al., 2022; Maharjan et al., 2022; Van Emmerik et al., 2020). Remote sensing detection also allows for measuring spectra beyond the RGB region captured by regular cameras, which is important for plastic detection as plastic absorption features occur outside this region (Tasseron et al., 2021). Controlled experiments help with understanding remote sensing plastic detectability. Research that used large artificial plastic targets has been done in the marine environment (Themistocleous et al., 2020; Topouzelis et al., 2020), but not in riverine environments. Image background, which is very different in riverine environments compared to marine environments, matters in plastic detection as it influences the spectral signal observed by the sensor (Michel et al., 2020; Olyaei & Ebtehaj, 2024; van Emmerik et al., 2022; Veettil et al., 2022). This means that riverine environments need to be researched separately.

A remote sensing method to upscale riverine plastic detection is multispectral camera detection. Multispectral cameras create images that, like satellite imagery, contain data beyond the RGB spectrum (Cortesi et al., 2022). Nowadays, an increase is visible in research on the automatic

detection of riverine plastics by using cameras (Anggraini et al., 2024). The use of multispectral cameras has shown potential when it comes to riverine plastic detection (Cortesi et al., 2022). De Giglio et al. (2021) found that the MAIA camera was effective in river plastic monitoring. The camera can be attached to a tripod or a UAV (Uncrewed Aerial Vehicle). UAVs are able to get close to the target and collect images at high resolution and frequency (Maharjan et al., 2022). This high resolution allows for the collection of pure multispectral plastic spectra. Spectral signatures of plastics are not always the same, as they differ between plastic types (Tasseron et al., 2021). The spectral signature of a plastic influences its detectability. Research on distinctive features in spectral signatures of plastics helps to understand how plastics can be detected (Tasseron et al., 2021). Multispectral MAIA S2 has the same spectral bands as Sentinel-2, except for bands 9, 10, 11, and 12, and thus provides information on how Sentinel-2 would measure a pure plastic spectrum (SAL Engineering et al., 2018). However, hyperspectral signatures contain more detail than multispectral signatures.

Another remote sensing method that has proven to be useful in plastic detection is satellite detection (Biermann et al., 2020; L. Schreyers et al., 2022). Biermann et al. (2020) proved for the first time that Sentinel-2 satellite imagery is effective for detecting floating macroplastic patches in the ocean. Sentinel-2 satellites are multispectral satellites with 12 bands covering a spectral range from the visible spectrum to the short-wave infrared (SWIR) spectrum (Copernicus EU & European Space Agency, n.d.). Sentinel-2 satellites have a spatial resolution of 10 m, 20 m, or 60 m depending on the satellite band, and a revisit time of 5 days. Monitoring coastal and inland waters is part of the mission of Sentinel-2 (European Space Agency, n.d.). The images are freely available, making it a potentially cost-effective method to detect plastic litter. Compared to Sentinel-2, PlanetScope images have a higher spatial resolution of approximately 3 meters and a higher revisit time of approximately one day (Planet Labs Inc., 2025). The spectral range of PlanetScope images covers the visible spectrum until the near infrared spectrum (NIR). PlanetScope is a commercial satellite, meaning the data is not free of charge. The PlanetScope images have eight bands, some of which are interoperable with Sentinel-2 (Figure 7, Appendix I, p.41). The EnMAP (Environmental Mapping and Analysis Program) satellite mission is developed and operated by the German Space Agency DLR in Bonn to monitor and characterise the Earth surface on a global scale (EnMAP, 2022). Scientific management is done by the German Research Centre for Geosciences (GFZ) in Potsdam. The satellite provides hyperspectral images with a spectral range of 420 nm to 2450 nm with intervals of 6.5 nm and 10 nm for the VNIR and SWIR bands. The ground resolution of the satellite is 30 meters, which is low compared to Sentinel-2 and PlanetScope. Comparing imagery of Sentinel-2, PlanetScope, and EnMAP allows for investigation of the trade-off between spectral and spatial resolution, which is relevant for plastic detection (Kremezi et al., 2022).

The aim of this study is to investigate how well plastics can be detected in riverbank environments across remote sensing sensors. This is done by means of a controlled field experiment. This research has the following research questions:

1) What are the distinctive features in spectral signatures that distinguish polyester and polyethylene terephthalate from river water and riverbank land covers across multispectral and hyperspectral sensors?

2) How do polyester and polyethylene terephthalate and their different cover sizes influence spectra measured by different satellite sensors?

3) What are detectable cover sizes of polyester and polyethylene terephthalate across remote sensing sensors?

Multispectral and hyperspectral signatures of a riverbank environment and two plastic types, polyester and polyethylene terephthalate (PET), were collected with the MAIA S2 and a handheld spectrometer. The spectral signatures are studied to identify features that differentiate the plastics from each other and the riverbank environment. Sentinel-2, PlanetScope, and EnMAP reflectance spectra of pixels containing different polyester and PET cover sizes are studied to determine the influence of the plastics and their coverage on these reflectance spectra. The most suitable sensor is used for further analysis. Then, ten spectral indices are analysed to determine their suitability for plastic detection, of which two spectral indices are used to determine detectability of the plastics across different cover sizes, by training a Naive Bayes model.

2. Data and methodology

To answer the research questions, a controlled field experiment was executed on a riverbank in March 2025. The experiment took two weeks, from 7 March until 21 March 2025. In those weeks, spectral signatures were collected in the field, and plastic targets were placed to collect satellite imagery. The size of the targets was changed to investigate plastic detectability.

2.1. Study area

The plastic targets were placed on the banks of the Nederrijn, one of the branches of the Rhine delta, near the city of Wageningen in the Netherlands (Figure 1, p.14). This location was chosen because it is large enough to place the plastic targets of the experiment (‘2.2 Plastic Targets’, p.12), it is easily reachable by car, and it is a relatively undisturbed area. Permission to construct and place the targets was obtained from Rijkswaterstaat by reporting the experiment and providing information in Omgevingsloket (on https://omgevingswet.overheid.nl/). In addition, permission was obtained from Rijksvastgoedbedrijf, which is the owner of the location. The water level in this part of the Nederrijn was expected to be quite stable as it is 11 kilometres downstream of a lock and weir complex in Driel that regulates the water level (Rijkswaterstaat, 2024b). To make sure the river did not flood the targets, the water information website of Rijkswaterstaat (Rijkswaterstaat, 2024a) was monitored two days in advance to see the predicted water level for the measurement location ‘Grebbe’ (which is closest to the fieldwork location). To ensure that the targets were not going to be damaged by the weather, e.g. by wind, the weather predictions were checked daily. The cloud cover during the field experiment was low, meaning two weeks was enough time to gather enough satellite data and to perform all the measurements.

2.2. Plastic targets

Two plastic targets were installed on the riverbank close to the water line. One of the targets was made of white polyester sheets, and the other target was made of transparent PET bottles attached to a net. To compare the detectability of different plastic cover sizes, the polyester target was decreased in size and the PET target was increased in bottle density. Although PET is part of the polyester family (Pang et al., 2006), the targets varied highly in colour (white versus transparent) and texture (fabric versus bottles). In the remainder of this report, the PET bottles will be referred to as PET and the polyester sheets will be referred to as polyester. Polyester fabric is commonly used as a textile, and PET is a specific polyester type that is very commonly used for packaging (Lechthaler et al., 2020; van Emmerik & Schwarz, 2020). In addition, white and transparent are the most common plastic colours in marine litter, which is supplied for a large part by rivers (Lebreton et al., 2017; Papageorgiou et al., 2022). Polyethylene and polypropylene are the most commonly produced plastic types (Lechthaler et al., 2020; van Emmerik & Schwarz, 2020), however these materials were not available for the field experiment. Both target types, their sizes (and the bottle densities), and the target placement with respect to the satellite pixels of the studied satellites (‘2.4 Satellite Imagery’, p.16) are shown in Figure 1 (p.14). In the experiment period, the state of the targets was checked three times a week.

2.2.1. The polyester targets

One of the target types was made from multiple polyester sheets that had sizes of 2 by 1 meters, 6 by 1 meters, or 10 by 1 meters. By placing these sheets next to each other, a large polyester target could be realised. By starting with a target size which was as large as possible and by using

a white colour, the chances of getting a satellite signal were maximised. The sheets were not stacked to maximise the target area, meaning the target consisted of a single layer of polyester sheets. Metal pins were used to pin the white sheets onto the subsurface. Stones were placed on the polyester sheets in places where no metal pins could be used because of the rocky subsurface. The stones covered only a very small part of the target, meaning their influence on the plastic signal was neglected. Data on the following polyester targets was collected:

- A 3 m x 30 m polyester target, deployed on 7 March
- A 2 m x 30 m polyester target, deployed on 9 March through 16 March
- A 1 m x 30 m polyester target, deployed on 17 March through 19 March
- A 0.5 m x 30 m polyester target, deployed on 20 March through 21 March

2.2.2. The PET bottle targets

The PET bottle targets consisted of 364 transparent PET bottles categorised in different sizes: Large (1.5 and 2 L), medium (1 L), and small (0.5 and 0.75 L). The bottles were attached to a black PE net with a mesh size of 100 x 100 mm^2 and a thread thickness of 1.3 mm. Metal pins were used to pin the net onto the subsurface. The bottles were attached to the net with a nylon thread. The vast majority of the bottles (> 95%) were transparent without colour, while only a very small fraction was transparent blue or transparent green. The influence of the colours was neglected because of the small fraction of coloured bottles. Per square meter, there was one large bottle and three medium bottles, or one large bottle, two medium bottles, and one small bottle. The two configurations were alternated. In the end, data was collected for two PET targets:

- A target of 3 m x 30 m with a PET bottle density of 4 bottles/m2, deployed on 9 March through 17 March
- A target of 3 m x 15 m with a PET bottle density of 8 bottles/m2, deployed on 18 March through 21 March

2.2.3. Target locations

The Topcon HiPer V GNSS receiver (Topcon Positioning Systems Inc., Livermore, California, USA) (Figure 8C, Appendix III, p.43) was used to measure the location of each plastic target with high accuracy. This was needed to determine the pixel coverage of the plastic targets within the satellite pixels. Multiple points along the outlines of the targets were measured, assuming a straight line between the points. The water line along the polyester target on 7 March was measured to use for the land cover map of the study area (discussed in '2.5.3 Naive Bayes classification', p.18).

The target placement was based on previous Sentinel-2 imagery. By choosing a length larger than 20 m and by placing the target at an angle compared to east-west and north-south alignment, chances were increased that the target crossed at least one pixel close to the pixel centre (most Sentinel-2 bands are 10 m or 20 m). Before placing the targets, the GPS coordinates of the ideal location were retrieved from previous Sentinel-2 images. The coordinates were tracked in the field by using the Topcon HiPer V GNSS Receiver. The targets were placed as close as possible to these coordinates, dependent on field conditions. For every satellite type studied, the target placement with respect to the satellite pixels is shown in Figure 1 (p.14).

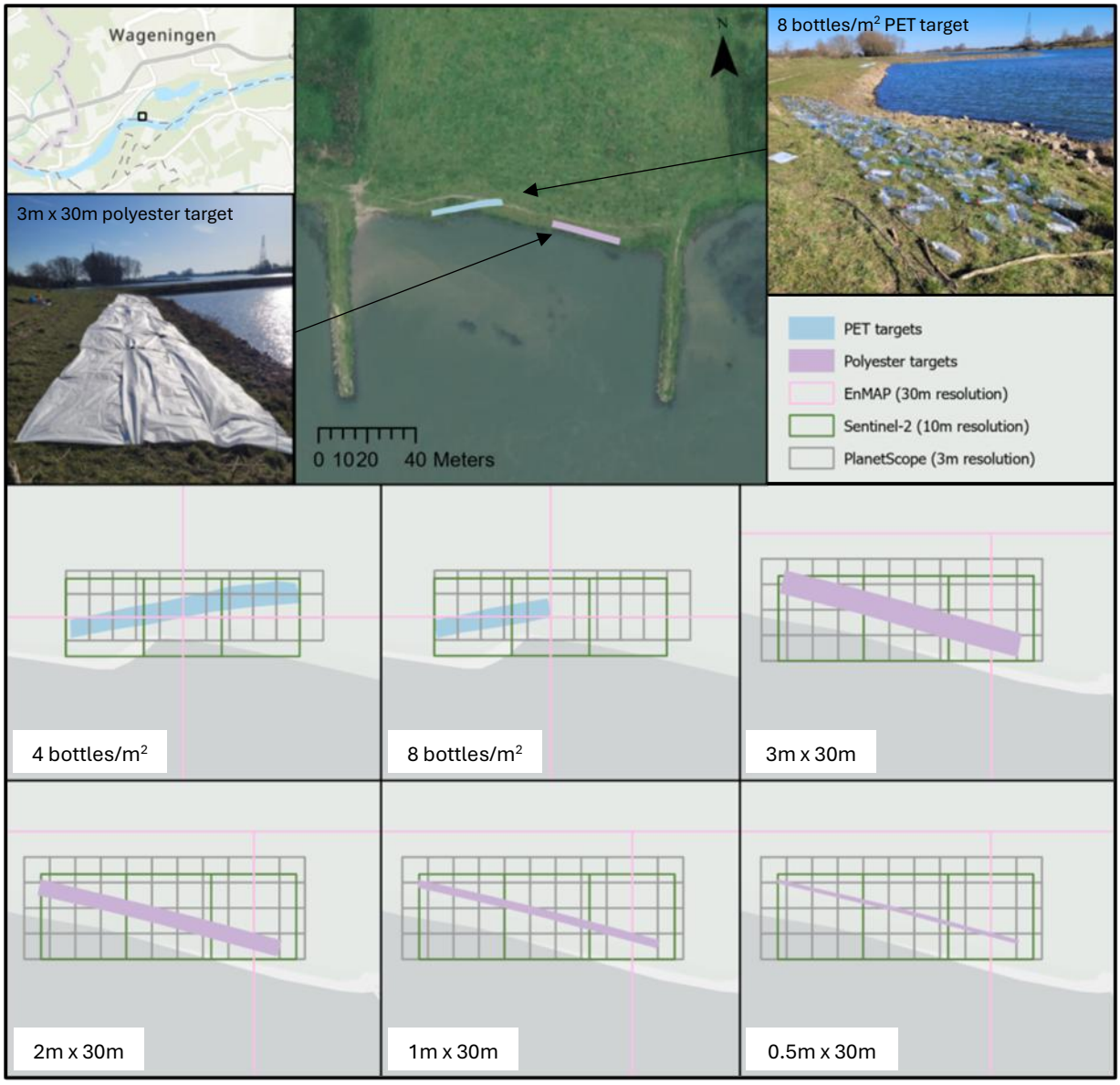

Esri, EsriNL, Rijkswaterstaat, Intermap, NASA, NGA, USGS; Esri Community Maps Contributors, Kadaster, Esri, TomTom, Garmin, GeoTechnologies, Inc, METI/NASA, USGS; Kadaster, Esri, TomTom, Garmin, METI/NASA, USGS; Sources: Esri, Maxar, Airbus DS, USGS, NGA, NASA, CGIAR, N Robinson, NCEAS, NLS, OS, NMA, Geodatastyrelsen, Rijkswaterstaat, GSA, Geoland, FEMA, Intermap, and the GIS user community

Figure 1 *Study area, plastic target locations and proportions, and plastic pixel coverage. The grids represent the outlines of the pixels in the images of EnMAP, Sentinel-2, and PlanetScope. For Sentinel-2, the 10 m pixels are shown.*

2.3. Spectral signatures

To determine the distinctive features in spectral signatures that differentiate polyester and PET from river water and riverbank land covers, hyperspectral and multispectral field measurements were done.

2.3.1. Hyperspectral measurements

The ASD Fieldspec Handheld 2 Spectroradiometer (HSR) (Malvern Panalytical, Malvern, Worcestershire, UK) (Figure 8B, Appendix III, p.43) was used to measure different spectra present in the study area and the spectra of polyester and PET. The following land covers were identified: Shrubs, grass, riparian vegetation, rock, water, sand, and soil (Table 4, Appendix II, p.42). During the experiment, it was discovered that the background had a large influence on the reflectance

spectra of polyester and PET. Multiple layers of polyester were stacked until there was no influence of the background anymore, so that the pure spectrum of polyester could be measured. The spectrum of one polyester layer on grass was used to analyse the spectrum of the polyester target in the field experiment. PET was measured on two different backgrounds, because these were the backgrounds of the PET target in the field experiment. The HSR had a range of 325 nm to 1075 nm, of which the range 400 nm to 900 nm remained after data pre-processing. There was no device available with a higher spectral range.

The person measuring held the HSR next to their body with their back turned to the sun to limit the influence of reflectance from their body on the measurement. The HSR was held at a predetermined height so that the field of view (FOV) of the instrument covered as much as possible of the land covers but as least as possible of the adjacent land covers. The sample count of the spectrum count averaging was set to 30. This was done for the white reference measurement, the dark current measurement, and the optimisation as well. During a measurement, the device was moved over the land cover. The black current-white reference measurement and the optimisation were done every 10 minutes or with shorter intervals when the lighting conditions or the slope of the measured land cover changed.

For each land cover, this was done at least three times on different locations within the study area. This increases the chance of getting a representative database of spectra for each land cover. Not all land covers were measured the same number of times, because of the investigative nature of this research and because of battery power issues of the device (Table 4, Appendix II, p.42).

2.3.2. Multispectral measurements

The MAIA S2 multispectral camera (Eoptis Srl., Trento, Italy; SAL Engineering, Russi, Italy) was used to create high-resolution images of the study area and the plastic targets from up close. These high-resolution images allowed for the analysis of pure pixels for each land cover and plastic type. The camera was placed on a 1.65 meter tall ladder. It was not allowed to use a drone in the study area during the field experiment. This would have made it possible to gather images that cover large parts of the study area at once, and at nadir. This was not possible by using the ladder, because the camera's field of view was too small to capture large areas.

The MAIA S2 camera was attached to a battery to enable power supply in the field (Figure 8A1, Appendix III, p.43). The voltage of the battery was continuously measured so that the battery would not run empty while the camera was still on. The camera was also attached to an Incident Light Sensor (ILS) (Figure 8A2, Appendix III, p.43). This sensor measured incoming atmospheric radiation as input for the radiometric correction of the MAIA S2 images. The top of the ILS had to be pointed upwards to correctly measure this. During data acquisition, automatic calibration was used to set the exposure times of the lenses.

2.3.3. Spectral signature analysis

The HSR and MAIA S2 allowed for the collection of pure land cover spectra. Their data was used to analyse the differences between the spectral signatures of the riverbank environment and the plastics.

The HSR data was imported from the instrument with the HH2 Sync software provided with the HSR. ViewSpec Pro was used to convert the .asd files of each spectrum to DAT files in which the spectra were stored per land cover. These DAT files were imported into a Python script for further preprocessing and analysis. To remove noise and increase data reliability, the spectra measured

with the HSR were first smoothed by using a Savitzky-Golay filter (Savitzky & Golay, 1964). Then the spectra were cropped to a wavelength range of 400 nm to 900 nm, because the values at the other wavelengths were very noisy. The smoothed spectra of the same land covers were taken together to calculate the mean spectrum and the standard deviation.

The reflectance spectra measured with the HSR were compared to the spectra collected with MAIA S2 to compare hyperspectral data to multispectral data. The MAIA S2 raw images were processed with the MultiCam Stitcher Pro v 1.4 software provided along with the camera. First, the raw images were previewed to select images without oversaturation. Then the raw files were converted to multilayer TIFF files after doing a radial correction, co-registration of the bands, and a radiometric correction by using the ILS data. These files were imported into ArcGIS Pro, in which polygons were created for each land cover to extract the reflectance values per land cover class. The mean and standard deviation of these values were calculated in Python. Only three images were used in the MAIA S2 analysis because of time constraints. One image was used from which the spectra of grass, riparian vegetation, rock, water, soil, and polyester were collected. Sand, shrubs, and PET were not (clearly) present in this image, so two additional images were used. A second image from which the spectra of sand and shrubs were collected, and a third image to collect the PET spectrum.

2.4. Satellite imagery

In the field experiment, images were acquired with three different satellite types. The properties of the satellites and their instruments are shown in Table 3 (Appendix I, p.41).

The first satellite type that was studied is Sentinel-2. At the time of the field experiment, Sentinel-2 contained three different generations that gathered data: Sentinel-2a, Sentinel-2b, and Sentinel-2c. This is an exceptional situation that occurred after the launch of Sentinel-2c (in September 2024), which is the replacement of Sentinel-2a, and after the Sentinel-2a campaign was extended by a year (Copernicus EU & European Space Agency, 2024, 2025). This means that during the field experiment, the revisit time of Sentinel-2 was increased compared to the usual 5 days. As these different generations collect nearly the same data, level 2A data from all the generations were used together in the analysis phase of this research.

PlanetScope data was accessed through a paid license by Wageningen University and Research. PlanetScope's SuperDove images were collected and the orthorectified and radiometrically corrected surface reflectance products were analysed, which are suitable for monitoring applications. During the field experiment, PlanetScope images were created on 11 days (of which six images were useful), meaning the revisit time was lower than the usual 1 day.

The third studied satellite type is the EnMAP satellite. Data acquisition for the study area in the fieldwork period was requested on the website of EnMAP (EnMAP, 2024). The data could be requested free of charge as it was for research purposes. First, it was needed to register in the EnMAP Instrument Planning Portal and to assign a user role. After this user role was accepted, a research proposal had to be submitted in which a topic description, the expiration date of the research, the research objectives, the methodology, and the expected results were described. After the proposal was approved, level 2A data with land processing was requested. The success of the acquisitions was dependent on the approval of EnMAP and the weather circumstances.

Because of the different revisit times of Sentinel-2 and PlanetScope, and the observation request process of EnMAP, the acquisition dates of the images varied. This also influenced how often certain targets were captured by each satellite. An overview of all the acquisitions in which clouds

did not cover the study area is given in Table 1. During the measurement period, six useful Sentinel-2 images, six useful PlanetScope images, and one useful EnMAP image were collected. For Sentinel-2 and PlanetScope, two additional images of the study area without plastic targets were used in the analysis as a baseline. One image was chosen right before the experiment period, and one image was chosen right after. The EnMAP observation request protocol did not allow for more useful images than one.

Table 1 *Images acquired with Sentinel-2, PlanetScope, and EnMAP. For each target, the date is shown on which a cloud-free image is acquired. For Sentinel-2 and PlanetScope, the dates are shown on which images were taken that are used in this research as a baseline scenario.*

Material	Size	Density	Sentinel-2	PlanetScope	EnMAP
Polyester	3x30 m	-	07/03/2025	-	-
Polyester	2x30 m	-	10/03/2025 12/03/2025* 14/03/2025*	15/03/2025* 16/03/2025	16/03/2025
PET bottles	3x30 m	4 bottles/m2	10/03/2025 12/03/2025* 14/03/2025* 17/03/2025	15/03/2025* 16/03/2025 17/03/2025	16/03/2025
Polyester	1x30 m	-	17/03/2025	17/03/2025 19/03/2025	-
PET bottles	3x15m	8 bottles/m2	20/03/2025	19/03/2025 20/03/2025 21/03/2025	-
Polyester	0.5x30 m	-	20/03/2025	20/03/2025 21/03/2025	-
No plastics	-	-	05/03/2025 24/03/2025	06/03/2025 27/03/2025	

*These images contained cloud shadow

2.4.1. Analysis of satellite spectra

Preprocessing and analysis of the satellite data were done in ArcGIS Pro and Python. All satellite data were collected as a surface reflectance product, meaning no additional pre-processing was needed except for cropping the images to the study area. Only cloud-free images were used, but there were two Sentinel-2 images and one PlanetScope image with cloud shadow. These images were used in the analysis to maximise the amount of data. The impact of the cloud shadow on the analysis was continuously reflected on.

To answer how polyester and PET and their different cover sizes influence spectra measured by the different satellite sensors, reflectance signals were retrieved from the pixels with the highest plastic coverages within the images. These reflectance signals measured by the different satellites of the different target sizes were analysed by visual inspection and comparison of absolute reflectance values.

2.5. Polyester and PET detection

The analysis of the satellite spectra led to the conclusion that the Sentinel-2 imagery collected in this study was most suitable for further analysis on polyester and PET detection. Because of time constraints, data from only one sensor could be investigated further. First, spectral indices were calculated for the study area to see which indices distinguish the plastic targets from the

environment. Next, Spearman correlation coefficients were calculated to find out whether the spectral indices could work as indicators for plastic coverages. Lastly, the two most important spectral indices were used for Naive Bayes classification to quantify the detectability of the plastic types and cover sizes. ArcGIS Pro and Python were used to execute the data analysis.

2.5.1. Spectral indices

Spectral indices were analysed that are used more often for plastic detection and that are used for differentiation between riverbank land covers (Table 5, Appendix IV, p.44-45). The indices were calculated from the Sentinel-2 images of the whole study area and the maps were analysed to determine the usefulness of each index for plastic detection. The most useful index, SI-13, and NDVI were used for the Naive Bayes classification (‘2.5.3. Naive Bayes classification’, p.18).

2.5.2. Relationship between polyester target size and spectral indices

It was investigated whether spectral indices could work as polyester target size indicators. For each Sentinel-2 image, the reflectance of the pixel with the highest polyester and PET coverage was converted to the spectral index values used in this research. For each spectral index, the Spearman correlation coefficient was calculated to analyse the relationship between the index value and the target sizes.

2.5.3. Naive Bayes classification

A Gaussian Naive Bayes model based on SI-13 and NDVI was trained and tested to analyse the detectability of the plastic targets more concretely. Data from 12 and 14 March was not used because of cloud shadow.

First, a land cover map was created in ArcGIS Pro to classify the satellite pixels. This was done for all satellites. The location of the plastic targets was measured with high accuracy by the Topcon. The other land cover classes in the land cover map were based on two 8cm RGB orthophotos of 2023 and 2024 (Beeldmateriaal Nederland, 2023, 2024), and photos made in the study area. The land cover map was converted to different classification rasters for each satellite type and plastic scenario. For each pixel, the land cover class was selected based on the land cover occurring at the centre of the pixel. This method was chosen based on the point spread function that causes satellites to capture the reflectance in the middle of a pixel better than the reflectance closer to the borders of the pixel (Kaiser & Schneider, 2008). The land cover classes of the pixels in which the plastic targets were present that were not yet defined as polyester or PET were changed to ‘polyester’ or ‘PET’. Riparian vegetation did not occur in the land cover map. Rock was taken out of the analysis as it covered only a small part of the study area and its location on the classification map was too uncertain.

The classification rasters were used to link the spectral index values of the pixels to the land covers in the study area. SI-13 and NDVI were plotted against each other to maximise class separability between the plastic classes and the other land cover classes. The mean, standard deviation, and the bounding box of each land cover class were calculated to be included in these plots. This was done for each sensor used in this study, so that the sensors could be compared. The plot belonging to Sentinel-2 was analysed more thoroughly. Plastic pixels were plotted as individual pixels to analyse the change of the spectral indices with plastic target size and density.

In addition, Naive Bayes models were trained and tested on this data to test whether it was possible to discriminate between the plastic pixels and the other land cover classes. This algorithm was chosen because of its good performance and suitability for small amounts of training data (Pedregosa et al., 2011). The GaussianNB function was used from the scikit-learn library in Python. The Naive Bayes algorithm was used in three different ways. Each time, SI-13 and NDVI were used as input features, and the Naive Bayes model was trained with two different sets of prior probabilities. The prior probability of a land cover is the probability that a pixel belongs to that land cover if no information about the SI-13 and NDVI values is given. The default prior probabilities of the Gaussian Naive Bayes model used in this research were based on the training sample sizes. Only 9 polyester pixels and 3 sand pixels were used for training, compared to 206 water pixels and 184 to 186 vegetation pixels (the amount depending on differences in PET target coverage between the images). This uneven sampling distribution had a large impact on the Naive Bayes. To eliminate the influence of the training sample sizes, Naive Bayes was also trained with equal priors for each class. The default priors were more realistic than the equal priors, because the chance of finding plastic in a riverbank environment is not equal to the chance of finding e.g. water. However, the default priors were not realistic for each riverbank pollution scenario, as this depends on the size of the study area and the severity of the plastic pollution. By using equal priors, there was no bias towards a specific land cover class.

In the first Naive Bayes method, the algorithm was trained on all available data to create probability distribution regions for each land cover. These regions showed for each combination of the two spectral index values, how high the chance is that a pixel would belong to a certain land cover class. The Naive Bayes algorithm was also trained on all data except for one polyester pixel on which was tested. This was done for each polyester pixel. In this method, the maximum amount of data was used for training while there was still one plastic pixel left for testing. Lastly, Naive Bayes was trained on all available images except for one image, which was used for testing. In this method, less data was used for model training, but on the other hand it was possible to analyse the classification of all land covers. Accuracy metrics were calculated, and confusion matrices were created to evaluate the classifications. The results of the three different Naive Bayes methods were compared to draw a conclusion on plastic detectability for different target sizes.

3. Results & Discussion

This research provides insight into how well plastics can be detected in riverbank environments across remote sensing sensors. In order to do so, the measurements from the field experiment were used in an analysis. This chapter provides the results and a critical discussion for each research question.

3.1. Analysing spectral signatures to differentiate polyester and PET from a riverbank environment

The multispectral and hyperspectral signatures of river water, riverbank, and the plastics were determined. By comparing these spectral signatures, the main characteristics of the spectra could be determined that distinguish plastics from the riverbank environment. Measurements from the HRS and the MAIA S2 were compared to determine which sensor is more suitable to differentiate plastic spectra from the riverbank environment (Figure 2).

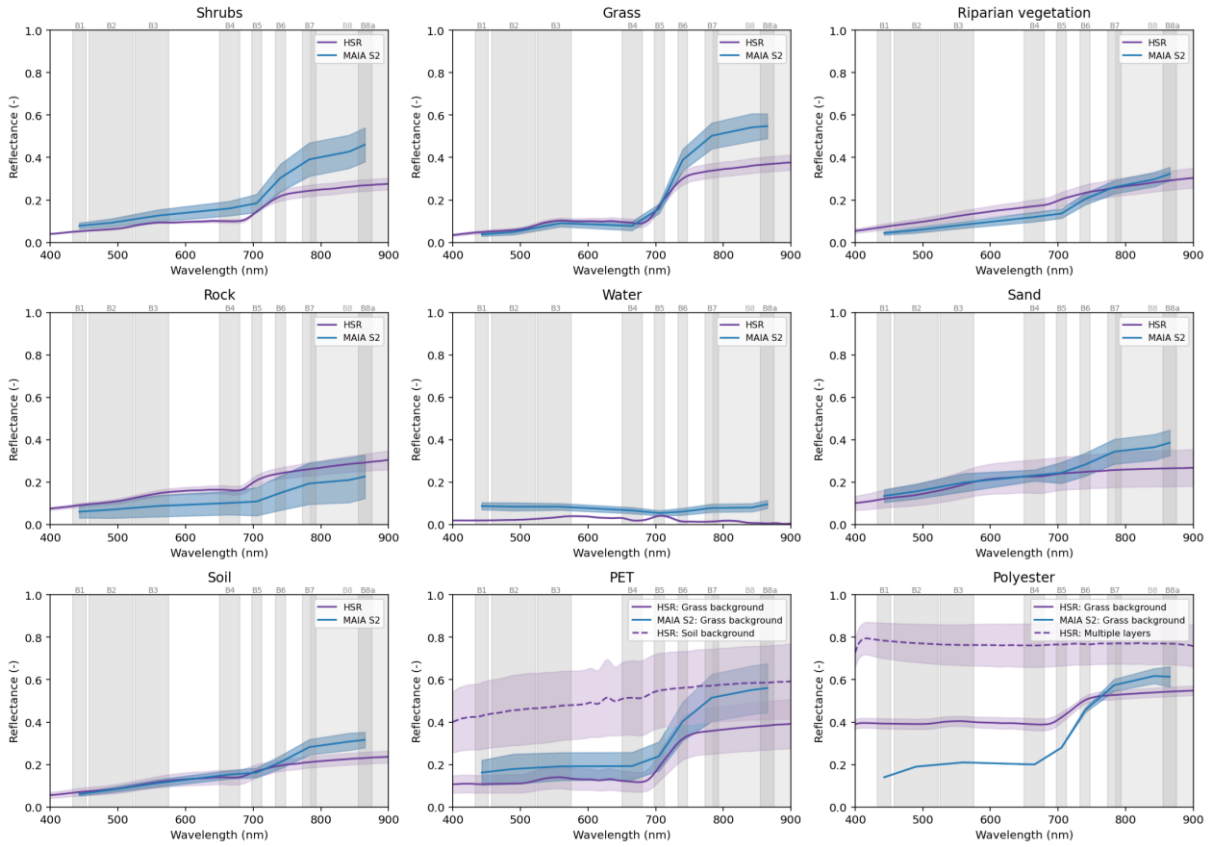

Figure 2 *The reflectance spectra of the main land covers in the study area, measured with the HSR and with MAIA S2. The HSR spectra range from 400 nm to 900 nm. The MAIA S2 spectra were interpolated between each band, covering a range from 433 nm to 875 nm. Each curve shows the mean spectrum of a land cover, with a shaded area around it representing the standard deviation of the land cover. HSR spectra were retrieved for PET on a soil background and on a grass background, because the PET target was lying both on soil and on grass. The polyester spectra that are described as 'Grass background' are the spectra of the polyester target from the field experiment. The target consisted of one layer of polyester lying on a grass background. The polyester spectrum that is described as 'Multiple layers' is the pure polyester reflectance measured from multiple stacked layers of polyester.*

Polyester is distinguishable in the HSR spectra by its higher reflectance compared to the other land covers. The HSR and MAIA S2 reflectance of the polyester target (indicated by 'Grass background') is influenced by the grass lying underneath the target, while the HSR spectrum of multiple layers of polyester is not influenced by this. For all wavelengths, polyester causes an increase in the reflectance of its background. The steep increase in the red edge and small peak in the green spectrum, typical for land vegetation (Ai et al., 2020; Seelig et al., 2008), are although diminished in the HSR spectrum, present in the polyester target spectrum. Between 400 nm and 680 nm the HSR polyester reflectance is approximately constant. This trend is different from the HSR spectra of the other land covers, in which reflectance is increasing in that area, except for water. The slight decrease in that area of the pure polyester spectrum (multiple layers) seems to diminish the increase in the grass spectrum. The MAIA S2 polyester spectrum does not have the same shape as the HSR spectrum. The MAIA S2 signal shows a lower value in band 1, which means the spectrum is more similar to the grass spectrum. Compared to MAIA S2, the HSR is better at measuring the differences between the polyester target spectrum and the grass spectrum. Additionally, the MAIA S2 measurements show very similar spectra for the polyester target and the PET target. There is a larger difference between the spectra measured by the HSR.

The spectrum of PET is highly influenced by its background, but has higher reflectance values in the RGB in the MAIA S2 spectra. HSR reflectance of PET on a grass background is only slightly higher than the reflectance of grass for wavelengths under 550 nm. The HSR spectrum of PET on a soil background is very similar to the spectrum of soil, except that the overall reflectance of the PET spectrum is higher. This is in line with Tasseron et al. (2021), who showed that transparent PET does not have any characteristic absorption features between 500 nm and 1700 nm (although the range between 850 nm and 950 nm was not analysed). Tasseron et al. (2021) hypothesised that this effect is caused by the transparency of the PET. The increase in reflectance caused by PET and the relatively high standard deviation of the PET reflectance (> 15%) is explained by the morphology of the PET bottles. Goddijn-Murphy & Dufaur (2018) found that reflectance is dependent on the shape of the measured object and the ambient light conditions. As only three measurements were done to determine the PET spectrum on a soil background and another three were done to determine the PET spectrum on a grass background, measuring different parts of the PET bottle in combination with the difference in rotation of the PET bottle relative to the sun, could have large effects on the increase in reflectance. Change in ambient light was taken into account by the black current-white reference measurements and the optimisation, but this does not account for the effect of the rotation of the PET bottle. The MAIA S2 is more suitable for the differentiation of the PET spectrum. MAIA S2 has an advantage over the HSR because it can capture large areas more easily, especially when attached to a UAV. The reflectance of many PET bottles, which have different rotations relative to the sun, can be captured at once. This means that there is a high chance that PET bottles will be measured that cause an increase in reflectance in the RGB. In addition, a higher variability in reflectance values can be measured, which differentiates the PET spectrum from many of the other spectra. The latter is relevant for the characterisation of the PET spectrum.

How the MAIA S2 data was collected influences the quality of the data. The MAIA S2 settings during data collection could explain the consistently increasing reflectance in the red edge and NIR compared to the HSR spectra. Automatic calibration was done to set the exposure time for each lens by using the ILS. The exposure times for the higher bands could be too high. In addition, the MAIA S2 images were taken under an angle which affects the absolute reflectance. The angle led to higher reflectance or lower reflectance compared to images taken at nadir (which is more common when using UAVs), depending on the position of the sun and topography. In case of

higher reflectance, PET bottles enhance this effect even more due to high scattering. This could explain the larger difference between PET reflectance and grass reflectance for MAIA S2 compared to the HSR measurements. In addition, the PET spectra were taken from a different image than the grass spectra. The images were taken under the same angle but not from the same perspective, which influenced absolute reflection. In short, this means that the absolute reflectance is not reliable. Despite this, conclusions can still be drawn from the shapes of the collected spectra. The effect of the angle can be diminished by looking at spectral indices that keep the shape of the reflectance curve, but do not take into account absolute reflectance. Still, it has to be taken into account that the MAIA S2 data is of low quality. In this research, there is no solid evidence presented that MAIA S2 can capture the increasing reflectance of PET bottles. However, the HSR has measured all wavelengths included in the MAIA S2 reflectance bands. When looking at PET bottles on a soil background, all wavelengths within the MAIA bands show increased reflectance for the HSR, making it likely that MAIA S2 can capture the increasing reflectance as well.

3.2. The influence of polyester and PET and their cover size on spectra measured by different satellite sensors

The influence of plastic type and cover size on spectra measured by Sentinel-2, PlanetScope, and EnMAP satellite sensors was studied. For each satellite type, the reflectance spectra of pixels with different polyester and PET coverages were compared visually. In the end, the most suitable sensor for further analysis was determined.

Polyester reflectance is increasing with target size in both the Sentinel-2 and PlanetScope reflectance spectra (Figure 3, p.23). In the Sentinel-2 spectra this happens in bands 2, 3, 4, and 5, and in the PlanetScope spectra in bands 1 through 7. It was decided that these bands would be important for polyester detection. The Sentinel-2 images taken on 12 March and 14 March, and the PlanetScope images taken on 15 March were affected by cloud shadow, which explains the divergent reflectance spectra on those dates. All the other images were cloud-free and thus provide more reliable reflectance values. It was not expected that the 0.5 m target could be detected, as all reflectance values are very close to the reflectance values of the scenario without a target. The same holds for all PET spectra. It was expected that 4b (4 bottles/m2) and 8b (8 bottles/m2) PET could not be detected in Sentinel-2 images. The transparency of the PET is a probable cause. Tasseron et al. (2021) hypothesised that the transparency of the PET causes a lack of characteristic absorption features that distinguish PET from its environment. Moreover, the combination with the low pixel coverage of the PET reduces chances of detectability further (Kremezi et al., 2022). Similarly, the PlanetScope PET reflectance spectra are very close to the scenario without a target, thus it was expected that PET could not be detected either.

For Sentinel-2, the relatively low reflectance in band 8 of the 8b spectrum and the lower reflectance values in band 11 of both the 8b and 4b spectra could not be logically explained, as the HSR measurements in Figure 2 (p.20) showed that PET should increase reflectance rather than decrease it. The patterns are likely based on other changing conditions, e.g. happening in the atmosphere or at sensor level. The peak reflectance in band 8 happening in both the polyester and the PET spectra is explained by the difference in spatial resolution between band 8 and its neighbouring bands. Band 8 has a high spatial resolution of ten meters, while other bands have a lower resolution of 20 or 60 meters. The plastic coverage within the ten meter pixel is higher than the coverage within the 20 meter or 60 meter pixels. As polyester increases the reflectance values of pixels, the ten meter resolution bands overall show higher reflectance values than they would

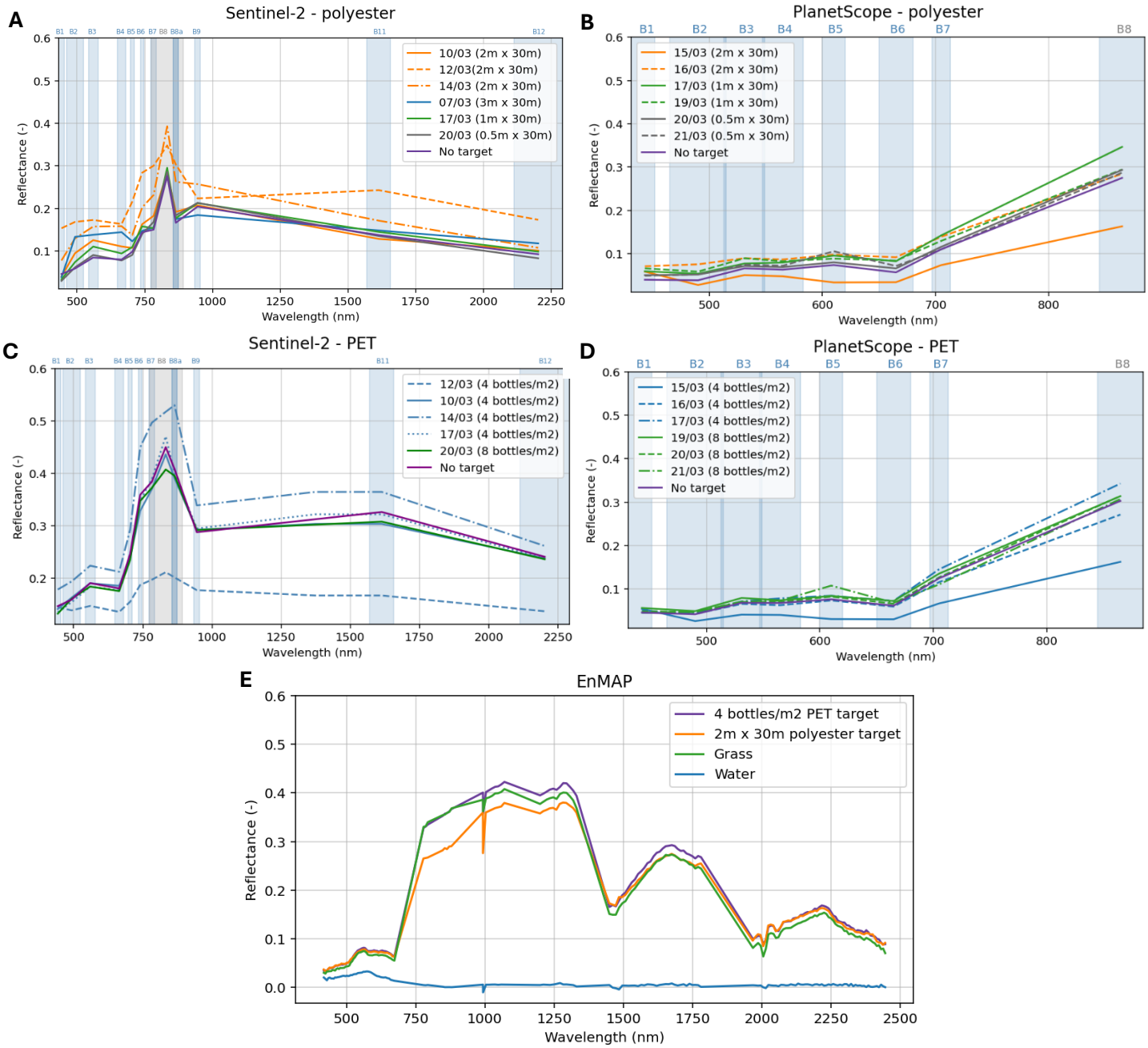

Figure 3 The reflectance spectra of different polyester and PET coverages for Sentinel-2, PlanetScope, and EnMAP. All spectra were taken from the satellite pixel in which the plastic coverage is highest. For Sentinel-2, the reflectance values were interpolated between the spectral bands to increase readability of the plot. However, Sentinel-2 bands have varying spatial resolutions, meaning that the interpolated values cannot be taken as true reflectance values. For Sentinel-2 and PlanetScope, the curves that are described as 'No target' are the average signals of two scenarios without plastic targets. Enlarged versions of Figures A and C can be found in Appendix V (p.46), as they are not entirely readable here. **A)** Sentinel-2 polyester reflectance for different target sizes. The 3 m, 2 m, 1 m, and 0.5 m polyester targets covered 29.6%, 19.7%, 10.1%, and 5.3% of the 10 m Sentinel-2 pixel respectively. **B)** Sentinel-2 PET reflectance for different target densities. The 4b PET target covered 7.1% of the 10m Sentinel-2 pixel. The 8b PET target covered 14.8%. **C)** PlanetScope polyester reflectance for different target sizes. The 2 m, 1 m, and 0.5 m polyester targets covered 64.4%, 34.1%, and 18.2% of the PlanetScope pixel respectively. **D)** PlanetScope PET reflectance spectra for different target densities. The 4b target covered 23.0% of the PlanetScope pixel, and the 8b target 42.2%. **E)** The reflectance spectra of the plastics, water, and grass retrieved with the EnMAP satellite. The entire polyester target fitted almost completely within one pixel, providing a pixel coverage of 5.5%. The other main land covers within the same pixel were water (59.2%) and grass (25.9%). The PET target was located at the intersection of three pixels. The reflectance of the pixel with the highest PET coverage (1.4%) is shown. The main land cover within this pixel was grass (96.0%).

have when they had a lower spatial resolution.

For PlanetScope, the polyester and PET spectra retrieved on 17 March show higher values in bands 7 and 8. The polyester and PET spectra retrieved on 21 March show a peak in band 5. These patterns are not related to the different plastic covers and can be explained by the low radiometric quality of PlanetScope compared to conventional satellites, such as Sentinel-2 (Dias et al., 2024; Latte & Lejeune, 2020). In addition, Sentinel-2 shows to capture the differences in signals between the polyester targets and the no-target scenario at least as good as PlanetScope. The maximum difference in absolute reflection between the target spectra and the no-target spectra within the bands important for polyester detection (bands 2, 3, 4, and 5 for Sentinel-2, and bands 1 through 7 for PlanetScope) of the 2 m target is 0.04 and for the 1 m target is 0.03 for both Sentinel-2 and PlanetScope. For the 0.05 m target this is 0.02 for Sentinel-2 and 0.01 for PlanetScope. Another benefit of Sentinel-2 is that it covers a larger spectral range than PlanetScope. This means Sentinel-2 seems more suitable for plastic detection than PlanetScope. The main advantage of PlanetScope is its high revisit time of one day. This makes image acquisition easier, which is especially beneficial at cloudy locations and in cloudy seasons. For comparison, PlanetScope images were made on 11 days in the experiment period, and Sentinel-2 images were made on 7 days, while Sentinel-2 image collection in the study period was more frequent than usual (‘2.4 Satellite imagery’, p.16).

There was only one useful image collected by the EnMAP satellite. Therefore, no robust conclusions can be drawn from this sparse data. The plastic and grass spectra (Figure 3E, p.23) are typical spectra of green vegetation (Ai et al., 2020; Seelig et al., 2008). Chlorophyll absorption bands are present around 400 nm and 650 nm. The dips around 1000 nm, 1200 nm, 1400 nm, 2000 nm, and 2500 nm are water absorption bands. The large water fraction within the polyester pixel explains the relatively low polyester reflectance between 680 nm and 1350 nm and could be causing the relatively large water absorption dip around 1000 nm.

It is probably not possible to detect the plastics in the EnMAP image, because of large similarities between the plastic spectra and the grass spectrum. The maximum difference in reflectance value between the grass and PET spectrum is 0.026. The reflectance values of the polyester target are mainly lower than those of grass, while spectral signatures of polyester show that it should have a higher reflectance than grass (Figure 2, p.20). The similarities are explained by the low plastic coverages within the EnMAP pixels (5.5% polyester coverage and 1.4% PET coverage). Moshtaghi et al. (2021) found that the absorption features of polyester are present around 1130 nm, 1171 nm, 1413 nm, and 1660 nm. These absorption features are not visible in Figure 3E (p.23). Additionally, in the PET spectrum there are no reflectance dips present between 1600 nm and 1700 nm as found by Tasseron et al. (2021). The absence of the absorption features verifies that the plastic coverages are too low for detection. The polyester target in the EnMAP image is one of the biggest targets of the experiment (the 2 m target). EnMAP reflectance is not influenced by this target, while the target shows to affect the reflectance values in the Sentinel-2 and PlanetScope spectra.

In this research, Sentinel-2 data is the most suitable option for plastic detection and will thus be used for further analysis. As mentioned, Sentinel-2 outperforms PlanetScope in radiometric quality, captures the reflectance change by polyester as least as good, and has a larger spectral range. The low spatial resolution of EnMAP proves to outweigh its ability to gather data at high spectral resolution, and the image acquisition process makes it hard to collect sufficient images for a proper analysis. However, EnMAP data can still be useful for the detection of large plastic pollution coverages of at least 100 m^2, such as those found at the Hidrovacas dam (> 10,000 m^2,

in Guatemala) and in the Nile River (Cerra et al., 2025). Especially since its high spectral resolution and range allow for the analysis of plastic absorption features (Schmidt et al., 2023).

3.3. Detecting polyester and PET in Sentinel-2 imagery

In the previous chapters, the main characteristics of the reflectance spectra were determined that distinguish plastics from the riverbank environment, and the most suitable satellite sensor for further analysis was determined: Sentinel-2. In this chapter, the detectability of plastic type and cover size in Sentinel-2 images was quantified. First, spectral indices were calculated for the study area to see which indices distinguish the plastic targets from the environment. Next, Spearman correlation coefficients were calculated to find out whether the spectral indices could work as indicators for plastic coverages. Lastly, the two most important spectral indices were used for Naive Bayes classification to quantify the detectability of the plastic types and cover sizes.

3.3.1. Spectral indices to differentiate plastics from a riverbank environment

Spectral indices were calculated from the Sentinel-2 imagery and mapped to assess which indices distinguish the plastic targets from the riverbank environment.

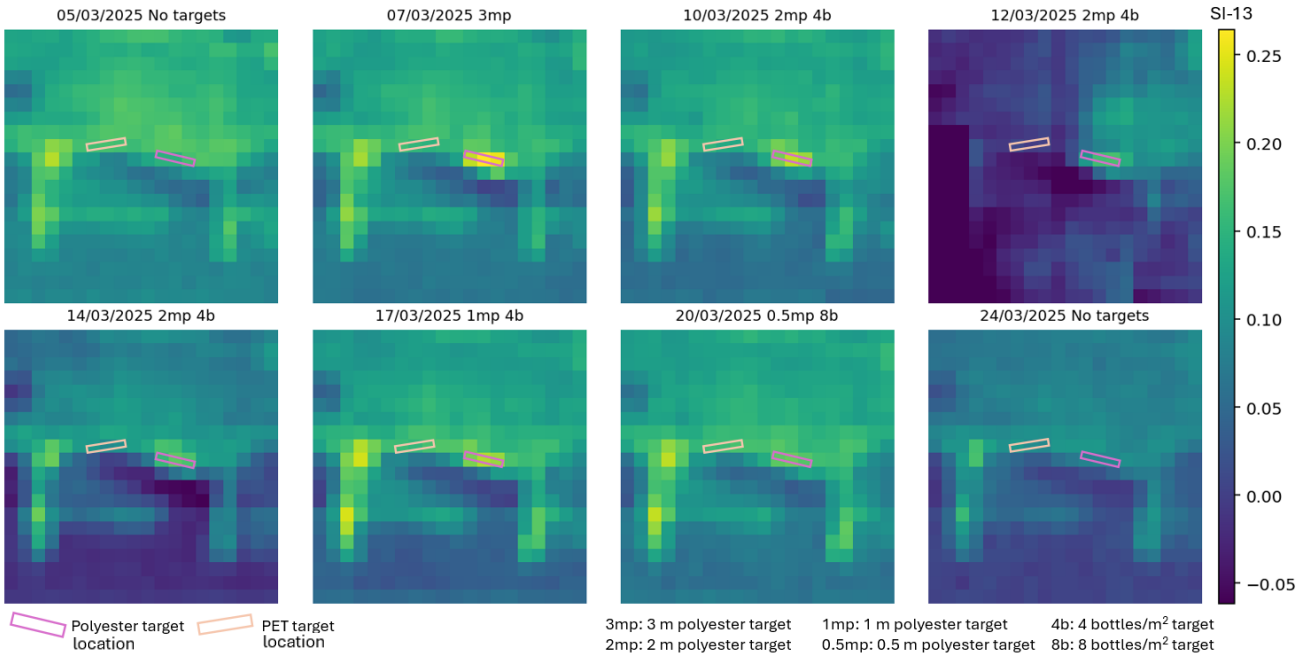

Figure 4 *SI-13 calculated for the Sentinel-2 images and mapped over the study area in chronological order. Locations of the plastic targets are indicated in each image to compare index values for different target coverages. In the image of the 3 m target, SI-13 is highest at the polyester target itself. This value is also the highest SI-13 value of all images. On 7, 10, and 12 March, one of the polyester pixels has the highest SI-13 value within the image. On 17 and 20 March, the SI-13 values that belong to the left groyne are higher than the values of the pixels belonging to the 2 m, 1 m, and 0.5 m polyester targets. The PET target did not influence the SI-13 values. The images of 12 and 14 March contain cloud shadow, which results in general in lower values. Since SI-13 represents the slope between two bands, this should have partly solved the cloud shadow issue. However, the results remain less reliable than for cloud-free images.*

SI-13 provides the best distinction between the polyester target and the riverbank environment and will be used for further analysis (Figure 4; the maps belonging to the other spectral indices can be found in Appendix VI, p.47-49). Polyester clearly shows high SI-13 values compared to the

environment, and the values are decreasing with decreasing target size. The FDI index was designed to detect floating debris on water, but it did not seem very effective for detecting polyester on land next to water. However, the 3 m polyester target influenced SI-23 with a much lower impact than SI-13, and the 2 m target did not have influence anymore. The PPI index reacts to the largest polyester cover, but a clear distinction from the environment purely based on this index was not possible. The API index seems to react to the polyester targets as well, but a clear distinction did not seem possible. NDVI did not provide a clear distinction between the plastic targets and their environment, which is in line with the spectral signatures measured with the HSR. Polyester increases reflectance values all over the spectral range, while keeping the slope in the red edge that is typical for vegetation and determines NDVI. This is applicable for NDWI, NDAVI, and PI as well.

None of the spectral indices calculated from the Sentinel-2 images seems to be affected by the PET targets (Figure 4, p.25; Figures 10-18, Appendix VI, p.47-49). This is in line with the spectral signature of PET, which is similar to the spectral signature of the background material. In addition, based on the Sentinel-2 reflectance spectra, it was concluded that the PET coverage in the experiment is too low to be detected.

3.3.2. Spearman correlations between spectral indices and plastic cover size

Spearman correlation coefficients were calculated to find out whether the spectral indices could work as indicators for plastic coverages. While the spectral index maps of the Sentinel-2 imagery in the previous chapter provide information about the separability of the plastic pixels from the other pixels in the riverbank environment, the correlation coefficients provide information about whether a spectral index can explain the width of the polyester target or the density of the PET target when looking at the plastic pixels specifically.

There is a clear correlation between every spectral index, except FDI and PGI, and the polyester target width, as the Spearman correlation coefficients are high and the p-values are under 0.05 (Table 2, p.27). NDAVI shows the highest correlation and results in a clear distinction between the 3 m target, 2 m target, and the no-target pixels (Figure 5, p.27). NDAVI, NDWI, NDVI, PI, and API are all based on the red edge slope starting at the visible spectrum and ending in the NIR. The HSR spectrum of polyester showed that polyester dampens the red edge slope of its grass background. This finding aligns with the idea that a higher polyester coverage dampens this red edge even more, influencing the aforementioned spectral indices. This effect is visible in the Sentinel-2 reflectance spectra as well (Figure 3A, p.23). The reflectance values of different target sizes are very similar in band 8, which represents the NIR. The bands in the RGB show increasing reflectance values with increasing target size. This means the red edge slope between the RGB and the NIR will decrease with increasing target size. The correlation coefficients of SI-13 and SI-23 are also in line with the Sentinel-2 reflectance spectra. These indices are based on the slopes between band 1 and the RGB region. The Sentinel-2 reflectance in band 1 remains stable with increasing target size, while the blue and green wavelengths show increasing reflectance with increasing target size.

There is no correlation found between the PET coverage and the spectral indices. SI-23 results in the highest correlation coefficient of -0.68 and a p-value of 0.095. As the p-value is above 0.05, it is concluded that there is no correlation. All other indices show p-values far above 0.05 and very low correlation coefficients.

NDVI will be used in combination with SI-13 to further analyse the detectability of the polyester targets. NDVI is a commonly used spectral index and has been proven to be useful in distinguishing between plastic target sizes.

Table 2 *Spearman correlation coefficients of the relationship between the plastic target size and the spectral indices calculated from Sentinel-2 imagery. For polyester, FDI and PGI show low correlation coefficients and p-values above 0.05, while the other indices show high correlation coefficients and p-values under 0.05. In particular, the correlation coefficients for NDAVI, NDWI, NDVI, PI, and API are very high. The correlation coefficients of SI-23 and SI-13 are very similar. The relationships between the spectral indices and the PET coverage have low correlation coefficients and p-values above 0.05.*

Spectral Index	Spearman correlation coefficient of polyester	P-value polyester	Spearman correlation coefficient of PET	P-value PET
NDAVI	-0.93	0.001	-0.12	0.799
NDWI	0.88	0.004	0.02	0.966
NDVI	-0.87	0.005	-0.14	0.766
PI	-0.87	0.005	-0.14	0.766
API	0.87	0.005	0.14	0.766
PPI	0.80	0.018	0.00	1.000
SI-23	-0.75	0.033	-0.68	0.095
SI-13	0.72	0.042	0.08	0.865
FDI	0.23	0.578	0.22	0.637
PGI	0.00	1.000	0.10	0.832

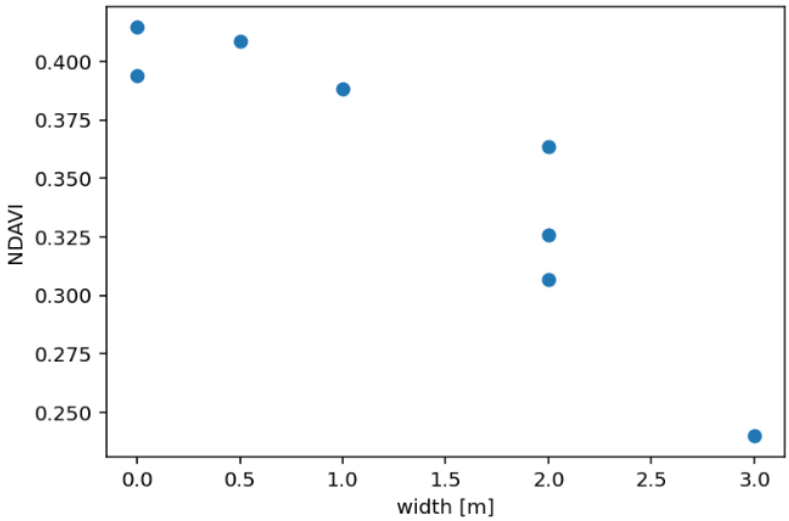

Figure 5 *The relationship between NDAVI values and polyester target width. The 2 m and 3 m targets clearly show a difference from each other and the no target scenario. The 1 m and 0.5 m targets do not show a (clear) difference.*

3.3.3. Naive Bayes classification to evaluate plastic detectability

SI-13 and NDVI were used for Naive Bayes classification to quantify the detectability of the plastic types and cover sizes. Three methods were used for Naive Bayes training and testing. In the first method, the Naive Bayes model was trained on all Sentinel-2 data and no data was left for testing. Thus, the maximum amount of data was used to determine the class probabilities in the best way possible (Figure 6, p.29). In the second method, Naive Bayes was trained on all pixels except for one polyester pixel, which was used for testing. This was done for each polyester pixel in the dataset. Lastly, a third method was used to get insight into the classification of all land covers. For this method, one image was used for testing while the other images were used for training. Each image was used for testing once. Appendix VII (p.50-52) contains an overview of the results of the second and third methods. PET was not used as input for the Naive Bayes models, because the PET targets were unlikely to be detected. Method 1 confirms this, as the PET pixel values fall within a region exhibiting a vegetation probability greater than 0.70.

There cannot be any conclusions drawn from the first method to determine whether a class would be predicted correctly, because all the data was used for training. The polyester pixels that are visualised on the class probabilities (Figure 6, p.29) were also used to determine these class probabilities. Nevertheless, it gives a good overview of the probability regions of each class. In addition, conclusions can be made based on the plastic pixels that do not fall within a region with high plastic probabilities, even though these pixels were used for training.

The centre and right 3 m polyester pixels are located outside all bounding boxes of the other land covers. This proves that the 3 m polyester target influences reflectance measured with Sentinel-2 in such a way that it can be distinguished from the land cover classes of the riverbank. The 3 m polyester target pixels have large SI-13 values, which are close to the area of the sand class. The left 3 m pixel even lies in the region exhibiting a high sand probability. The smaller the size of the polyester target, the lower SI-13 and the higher NDVI. This means that the index values get closer to those of the vegetation class. It becomes clear that the 0.5 m target cannot be detected when the default priors are used, as its values fall within a region exhibiting a vegetation probability greater than 0.70. For the equal prior Naive Bayes model, the 0.5 m target falls in a region with a polyester probability greater than 0.70.

The plots that combine SI-13 and NDVI for the measurements of the other sensors used in this research (Figure 21, Appendix VII, p.53) show that the plastic pixels are not clearly separable from the other land cover classes, except for the data from the HSR. In addition, the HSR shows the ability to distinguish between PET and the other land covers. The HSR is better at detecting plastics because the measurements represent pure plastic spectra instead of mixed pixels. In the HSR plot, polyester has the lowest NDVI value, which is different compared to the Sentinel-2 results in which water has the lowest NDVI values. This is because the HSR measurements of water were taken at shallow locations, meaning the river bottom could be influencing the measurements.

The second method, in which Naive Bayes was trained on all data except for one polyester pixel which was used for testing, used the maximum amount of available good-quality data for training. Two-thirds of the 3 m polyester pixels, all 1 m polyester pixels, and all 2 m polyester pixels were classified correctly (Tables 6-7, Appendix VII, p.50). The left 3 m polyester pixel was misclassified as sand. Using the model with default priors, two-thirds of the 0.5 m polyester pixels were classified correctly. The right pixel of the 0.5 m target was classified as vegetation. Using the model with equal priors, the full 0.5 m target was classified as vegetation.

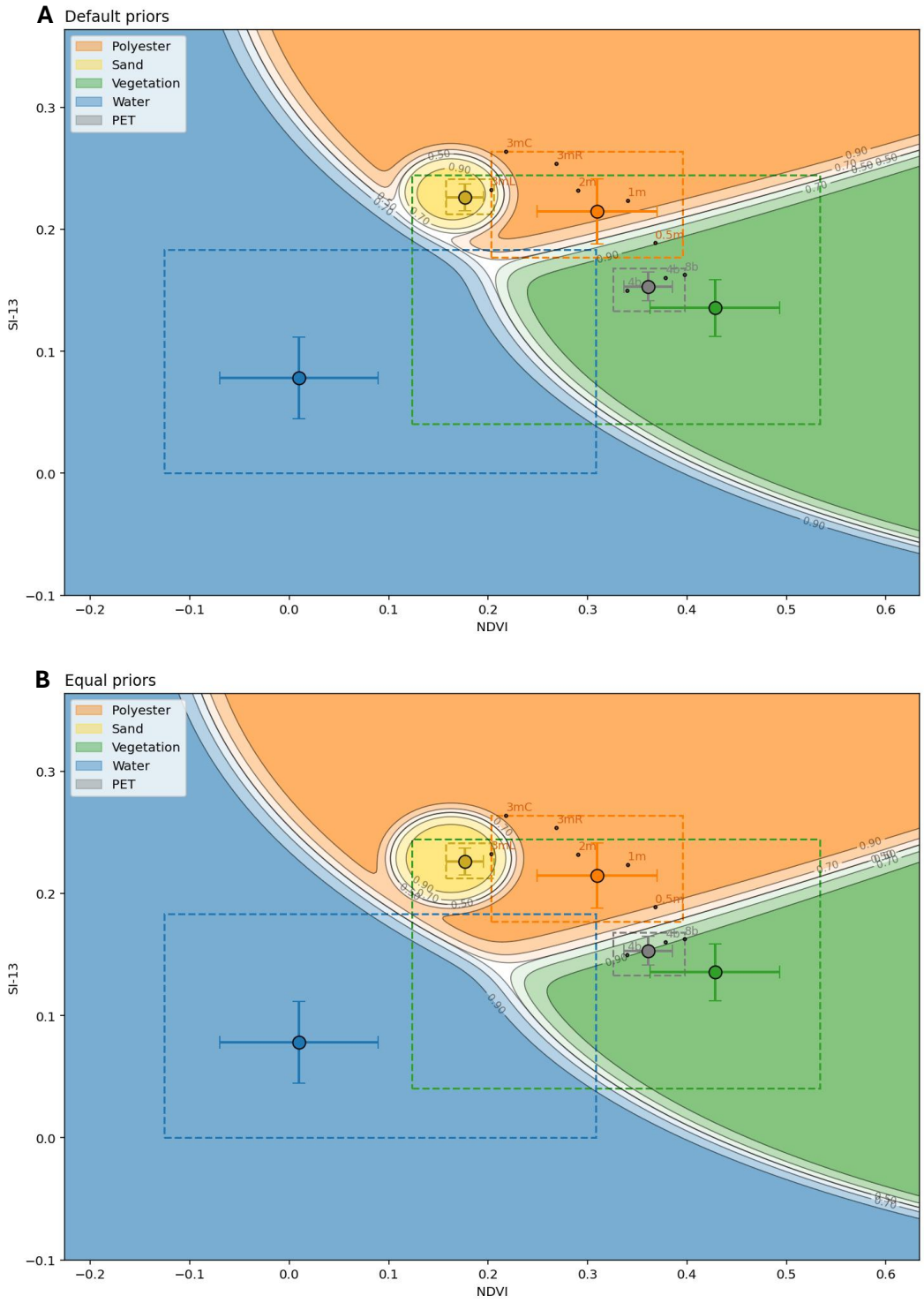

Figure 6 *Naive Bayes class probabilities and distributions of the classified Sentinel-2 pixels. SI-13 and NDVI are combined to increase separability between the plastics and the other land covers in the study area. For each land cover, the mean and standard deviation are shown. The bounding boxes delineate the ranges of the pixel values within each land cover. Because the shrub land cover has very similar SI-13 and NDVI values as grass, this land cover was taken together with grass into the combined vegetation land cover. The polyester and PET (4b = 4 bottles/m², 8b = 8 bottles/m²) pixels with the highest plastic coverages in each image are shown. All pixels covered by the 3 m polyester target are shown (3mL = left pixel, 3mC = centre pixel, 3mR = right pixel). The probability distribution, resulting from training the Naive Bayes model on all four cloud-free Sentinel-2 images, is shown as shaded regions.* ***A)*** *Naive Bayes model trained with the default prior probabilities, aligning with the sample size of the training data.* ***B)*** *Naive Bayes model trained with equal prior probabilities for each class. The equal priors give a higher priority to the polyester and sand classes, as these classes are underrepresented in the training data.*

In the third method, in which Naive Bayes was trained and tested on different images, less data is used for model training. However, this method provides information about the classification of all land covers (Tables 8-9, Figures 19-20, Appendix VII, p.51-52). The recall of the 3 m target is 0.33, meaning one-third of the 3 m pixels was classified correctly. The recall values of the 2 m and 1 m targets are both 1.00, meaning all target pixels were classified correctly. The recall of the 0.5 m target depends on the prior probabilities and is 0.00 for default priors and 0.67 for equal priors. The misclassified 3 m pixels were classified as sand, and the misclassified 0.5 m pixels were classified as vegetation. All precision and F-score values are 0.5 or lower, except for the F1-score of the 2m target when using default priors (which is 0.60). This is caused by the small number of polyester pixels compared to the number of pixels of some of the other classes. In the confusion matrices it can be seen that a maximum of 12 pixels were misclassified as polyester (Figures 19-20, Appendix VII, p.52). This is a large amount compared to the amount of plastic pixels, but a small amount compared to the total amount of pixels used for testing, which is around 395. The overall accuracy scores of the image classifications are 0.94 or higher, meaning most of the pixels were still correctly classified even when using equal prior probabilities. The Naive Bayes model with equal priors classified more polyester pixels correctly than the Naive Bayes model with default priors, but more pixels of other land covers were misclassified as polyester.

The 1 m, 2 m, and 3 m polyester targets can be detected in the riverbank environment. Methods 2 and 3 always showed a correct classification for at least one of the 3 m polyester pixels. All three pixels of the 1m target and the 2m target were classified correctly in methods 2 and 3. The 0.5 m target can be detected with the equal prior model, but not with the default prior model. The misclassified pixels were classified as vegetation, which is the background land cover of the target. This means the background signal was getting more dominant over the polyester signal. For equal priors, the target was partly classified correctly, but this scenario is less realistic than for default priors. In addition, all three methods include a location bias as data was used from the same study area. This led to overfitting of the models on the study area, making it easier for the models to predict the land covers correctly. Besides, the images were taken within a period of 2 weeks, meaning the model is biased towards a specific season. These biases, together with the poor results of the default prior model, make it unclear whether the 0.5 m target will be detected when using more qualitative models and more data.

Classification of pixels with a high polyester coverage as sand is partly because an increasing polyester coverage leads to a lower NDVI approaching the low NDVI of sand, but also because of the SI-13 index. The SI-13 index is based on band 1 and band 3, which both have a different spatial resolution of 60m and 10m respectively. Band 1 showed to be rather consistent with target size, which makes sense as the target covers are very low within the 60 by 60 meter pixels and the same pixel was used for each target size spectrum. Band 3 reflection shows a clear increase with target size, which is possible because of the high polyester coverage within the ten meter pixel used for this band. This means SI-13 is capturing the increasing reflectance in the RGB compared to a rather constant reflectance in the direct environment of the target which is relatively low because of the low influence of polyester. Reflectance in band 1 is dependent on aerosol concentration, meaning a changing aerosol concentration will lead to changing reflectance values in band 1 (Copernicus EU & European Space Agency, n.d.). During the field experiment these conditions were comparable for each image because they were taken within a short time period of two weeks and with comparable atmospheric conditions. The sand beach in the study area has an area of order of magnitude 100 m^2 which is close to the target area of the 3 m target, which is 90 m^2. In Addition, the sand beach has a high reflectance compared to the surrounding grass and water as well. This means that the sand beach is likely to cover a large part of the 10 meter pixel of the green

band and a small part of the 60 meter pixel of band 1. This will result in high SI-13 values as the reflection in band 3 is relatively high. This difficulty of SI-13 would arise each time there is a land cover with a high reflectance compared to its surroundings. Although for riverbank environments that consist primarily out of grass the SI-13 index can be a useful tool, but it would be more logical to use band 3 only, especially when looking at other devices than Sentinel-2. In Figure 21 in Appendix VII (p.53) it can be seen that the SI-13 index is not useful for the other devices as these do collect data at different spatial resolutions.

Overall, the findings of this study showed that plastic detection by using Sentinel-2 imagery is possible for polyester targets as small as 1m by 30 m. In the next section, the main results are summarised and reflected upon to form a conclusion for the entire research. As a closing, recommendations are made for further research.

4. Conclusion

This paper demonstrates that plastic detection in riverbank environments by using satellite and camera imagery is feasible and should be investigated further. A controlled field experiment in which plastic targets were placed on the riverbanks of the Nederrijn was executed successfully. The collected data was used to determine the spectral signatures of the riverbank environment and the plastics, to determine the influence of plastic type and cover size on satellite spectra measured by different satellite sensors, and to quantify the detectability of different plastic types and cover sizes in Sentinel-2 imagery.

Spectral signatures of riverbank, river water, and plastics can be distinguished visually. Although PET is part of the polyester family, the PET bottle target and the polyester sheet target showed different characteristics in their spectral signatures. Transparent PET is hard to distinguish from the other land covers as its spectrum is similar to the spectrum of its background. Depending on the shape and placement of the PET object, and on the lighting conditions, PET could lead to an overall increased reflectance. Therefore, PET pixels showed larger standard deviations compared to the other land covers. White polyester sheets can mainly be distinguished based on a high overall reflection compared to the spectra of the other land covers. The polyester spectra are also influenced by the background material during reflectance measurements, but polyester more strongly increases the overall reflection than PET and changes the reflectance in the 400 nm and 680 nm range. The hyperspectral HSR measurements resulted in larger differences between the polyester target and grass compared to the multispectral MAIA S2 measurements, while the MAIA S2 was more suitable to measure PET.

In this study, Sentinel-2 data is preferred over PlanetScope data for plastic detection because, although PlanetScope images have a higher spatial resolution, they did not prove to be more useful than Sentinel-2 images. Additionally, Sentinel-2 has a higher radiometric quality and has a larger spectral range. Sentinel-2 spectra were found to be influenced by the 3 m, 2 m, and 1 m polyester targets in bands 2, 3, 4, and 5. PlanetScope reflectance spectra were influenced by the polyester targets in bands 1 through 7. There was no influence of the PET targets on the spectra of Sentinel-2 and PlanetScope. The spatial resolution of EnMAP is too low to detect the plastics in the field experiment. However, EnMAP could still be useful to detect high amounts of plastic pollution that cover large areas.

In this research, the 1 m, 2 m, and 3 m polyester targets were detected in Sentinel-2 imagery by using Naive Bayes classification. All 1 m and 2 m pixels were classified correctly, and for every model run at least one of the 3 m target pixels was correctly classified. PET was not used for training the Naive Bayes model, as the targets did not influence the reflectance spectra of Sentinel-2. In addition, the PET pixel values had a probability greater than 0.70 of being classified as vegetation. A large part of the analysed spectral indices were found to be indicators of plastic cover size in Sentinel-2 imagery. The largest correlation between spectral index value and polyester target width was -0.93, for NDAVI.

Remote sensing plastic detection is a developing discipline that is very promising and shows a lot of possibilities. Recommendations are made in the next chapter to enhance research on plastics detection in riverbank environments across remote sensing sensors.

5. Recommendations

This paper serves as a proof of concept to show that plastic detection in riverbank environments by using satellite and camera imagery is feasible and should be investigated further. The data gathered in this research and used for analysis were sparse. More data collection is needed to build qualitative classification models. To achieve this, more controlled field experiments could be carried out to analyse different plastic types, target sizes, and riverbank environments. Plastic types that could be investigated are polyethylene and polypropylene, as they are the most produced plastic types (as mentioned in '2.2 Plastic targets', p.12). In addition, a focus on targets consisting of more realistic plastic waste, like the PET target, and combined plastic types would lead to a better understanding of detecting real plastic pollution. The type of riverbank environment has a large influence on detectability, which should be taken into account. It is recommended to place the plastic targets at different locations for each image and to compare the influence of the different seasons on the land cover spectra, as these factors introduced a bias in the used model. Another way to gather more data is to analyse existing plastic pollution patches in riverbank environments by using satellite and camera imagery. Gathering information on the plastic composition and size of the patches together with the satellite and camera analysis leads to a better understanding of what plastic waste and compositions can be detected.

It is recommended to use Sentinel-2 data in further research on plastic detection, as this data proved to be useful in detecting plastics. The main advantage of using satellite data is that plastic detection can be upscaled to a global scale. This can be combined with field detection on a local scale. For detection on a local scale, it is recommended to use hyperspectral cameras mounted on a UAV. The hyperspectral camera combines the high spatial resolution of the MAIA S2 with the high spectral resolutions of EnMAP and the HSR. By mounting the camera to an UAV, large areas can be covered.

Investigation of more spectral signatures of riverbanks and other plastic types is recommended. In addition, the limited spectral range of the HSR limits the comparison between the spectral signatures of the land covers. Reflectance values for higher wavelengths may show important differences relevant for the Sentinel-2 and EnMAP analysis. Measuring reflectance from 400 nm to 2450 nm in future experiments would lead to a higher quality analysis. In this research it was not possible because there was no suitable device available.

Finally, there was not enough time to consider other classification models than the Naive Bayes model. When Naive Bayes is used again, a more thorough analysis on the prior probabilities of the classes is needed as these have a large impact on the results. In addition, different models could be compared to classify plastics. Automated machine learning models applied on Sentinel-2 imagery, such as Random Forest, Support Vector Machine, and K-means models proved to be effective for plastic detection in coastal waters (Danilov & Serdiukova, 2024). However, more research is needed on what models are effective for plastic detection in riverine environments.

References

Ai, S., Zheng, H., & Yu, J. (2020). Preparation and reflectance spectrum modulation of Cr2O3 green pigment by solution combustion synthesis. *Materials*, *13*(7). https://doi.org/10.3390/ma13071540

Anggraini, N., Tawakkal, I., Akrim, D., Rachman, I., & Matsumoto, T. (2024). Visual Observation to Detect Macroplastic Object in River: A Review of Current Knowledge. *Journal of Community Based Environmental Engineering and Management*, *8*(8), 93–102. https://doi.org/10.23969/jcbeem.v8i1.12254

Beeldmateriaal Nederland. (2023). *Luchtfoto 2023 Ortho 8cm RGB*. Publieke Dienstverlening Op de Kaart. https://www.pdok.nl/ogc-webservices/-/article/pdok-luchtfoto-rgb-open-

Beeldmateriaal Nederland. (2024). *Luchtfoto 2024 Ortho 8cm RGB*. Publieke Dienstverlening Op de Kaart. https://www.pdok.nl/ogc-webservices/-/article/pdok-luchtfoto-rgb-open-

Biermann, L., Clewley, D., Martinez-Vicente, V., & Topouzelis, K. (2020). Finding Plastic Patches in Coastal Waters using Optical Satellite Data. *Scientific Reports*, *10*(1). https://doi.org/10.1038/s41598-020-62298-z

Breukel, R. (2025). *Spotting river plastic hotspots from space [Bsc. thesis]*.

Cerra, D., Auer, S., Baissero, A., & Bachofer, F. (2025). Detection and Monitoring of Floating Plastic Debris on Inland Waters From Sentinel-2 Time Series. *IEEE Journal of Selected Topics in Applied Earth Observations and Remote Sensing*, *18*, 1122–1138. https://doi.org/10.1109/JSTARS.2024.3502796

Copernicus EU, & European Space Agency. (n.d.). *S2 Mission*. Retrieved June 10, 2025, from https://sentiwiki.copernicus.eu/web/s2-mission

Copernicus EU, & European Space Agency. (2024, September 5). *Sentinel-2C launch*. https://sentinels.copernicus.eu/-/sentinel2-c-launch

Copernicus EU, & European Space Agency. (2025, February 28). *Sentinel-2A: Extended Campaign Starting March 13, 2025*. https://sentinels.copernicus.eu/web/sentinel/-/sentinel-2a-extended-campaign-starting-march-13-2025

Cortesi, I., Masiero, A., Tucci, G., & Topouzelis, K. (2022). UAV-BASED RIVER PLASTIC DETECTION WITH A MULTISPECTRAL CAMERA. *International Archives of the Photogrammetry, Remote Sensing and Spatial Information Sciences - ISPRS Archives*, *43*(B3-2022), 855–861. https://doi.org/10.5194/isprs-archives-XLIII-B3-2022-855-2022

Danilov, A., & Serdiukova, E. (2024). Review of Methods for Automatic Plastic Detection in Water Areas Using Satellite Images and Machine Learning. In *Sensors* (Vol. 24, Issue 16). Multidisciplinary Digital Publishing Institute (MDPI). https://doi.org/10.3390/s24165089

De Giglio, M., Dubbini, M., Cortesi, I., Maraviglia, M., Parisi, E. I., & Tucci, G. (2021). Plastics waste identification in river ecosystems by multispectral proximal sensing: a preliminary methodology study. *Water and Environment Journal*, *35*(2), 569–579. https://doi.org/10.1111/wej.12652

Dias, R. L. S., Amorim, R. S. S., da Silva, D. D., Fernandes-Filho, E. I., Veloso, G. V., & Macedo, R. H. F. (2024). Relative Radiometric Normalization for the PlanetScope Nanosatellite Constellation Based on Sentinel-2 Images. *Remote Sensing*, *16*(21). https://doi.org/10.3390/rs16214047

EnMAP. (2022). *Environmental Mapping and Analysis program: Mission overview and applications*. https://www.enmap.org/data/doc/Web_EnMAP_komplett_2022_eng.pdf

EnMAP. (2024, December 11). *Data & Access*. https://www.enmap.org/data_access/

European Space Agency. (n.d.). *Sentinel-2 operations*. Retrieved June 10, 2025, from https://www.esa.int/Enabling_Support/Operations/Sentinel-2_operations#:~:text=The%20mission&text=It%20is%20also%20monitoring%20coastal,once%20both%20are%20in%20orbit

Planet Labs Inc. (2025, May 5). *PlanetScope*. https://docs.planet.com/data/imagery/planetscope/

Fritz, S., See, L., & Grey, F. (2022). The grand challenges facing environmental citizen science. In *Frontiers in Environmental Science* (Vol. 10). Frontiers Media S.A. https://doi.org/10.3389/fenvs.2022.1019628

Gall, S. C., & Thompson, R. C. (2015). The impact of debris on marine life. *Marine Pollution Bulletin*, *92*(1–2), 170–179. https://doi.org/10.1016/j.marpolbul.2014.12.041

Gallitelli, L., Cesarini, G., Cera, A., Sighicelli, M., Lecce, F., Menegoni, P., & Scalici, M. (2020). Transport and deposition of microplastics and mesoplastics along the river course: A case study of a small river in central Italy. *Hydrology*, *7*(4), 1–16. https://doi.org/10.3390/hydrology7040090

Gallitelli, L., Cutini, M., Cesarini, G., & Scalici, M. (2024). Riparian vegetation entraps macroplastics along the entire river course: Implications for eco-safety activities and mitigation strategies. *Environmental Research*, *263*. https://doi.org/10.1016/j.envres.2024.120224

Goddijn-Murphy, L., & Dufaur, J. (2018). Proof of concept for a model of light reflectance of plastics floating on natural waters. *Marine Pollution Bulletin*, *135*, 1145–1157. https://doi.org/10.1016/j.marpolbul.2018.08.044

Hauk, R., van Emmerik, T. H. M., van der Ploeg, M., de Winter, W., Boonstra, M., Löhr, A. J., & Teuling, A. J. (2023). Macroplastic deposition and flushing in the Meuse river following the

July 2021 European floods. *Environmental Research Letters*, *18*(12). https://doi.org/10.1088/1748-9326/ad0768

Kaiser, G., & Schneider, W. (2008). Estimation of sensor point spread function by spatial subpixel analysis. *International Journal of Remote Sensing*, *29*(7), 2137–2155. https://doi.org/10.1080/01431160701395310

Kremezi, M., Kristollari, V., Karathanassi, V., Topouzelis, K., Kolokoussis, P., Taggio, N., Aiello, A., Ceriola, G., Barbone, E., & Corradi, P. (2022). Increasing the Sentinel-2 potential for marine plastic litter monitoring through image fusion techniques. *Marine Pollution Bulletin*, *182*. https://doi.org/10.1016/j.marpolbul.2022.113974

Latte, N., & Lejeune, P. (2020). PlanetScope radiometric normalization and sentinel-2 super-resolution (2.5 m): A straightforward spectral-spatial fusion of multi-satellite multi-sensor images using residual convolutional neural networks. *Remote Sensing*, *12*(15). https://doi.org/10.3390/RS12152366

Lebreton, L. C. M., Van Der Zwet, J., Damsteeg, J. W., Slat, B., Andrady, A., & Reisser, J. (2017). River plastic emissions to the world's oceans. *Nature Communications*, *8*. https://doi.org/10.1038/ncomms15611

Lechthaler, S., Waldschläger, K., Stauch, G., & Schüttrumpf, H. (2020). The way of macroplastic through the environment. In *Environments - MDPI* (Vol. 7, Issue 10, pp. 1–30). MDPI AG. https://doi.org/10.3390/environments7100073

Ledieu, L., Tramoy, R., Mabilais, D., Ricordel, S., Verdier, L., Tassin, B., & Gasperi, J. (2022). Macroplastic transfer dynamics in the Loire estuary: Similarities and specificities with macrotidal estuaries. *Marine Pollution Bulletin*, *182*. https://doi.org/10.1016/j.marpolbul.2022.114019

Lee, J., Hong, S., Song, Y. K., Hong, S. H., Jang, Y. C., Jang, M., Heo, N. W., Han, G. M., Lee, M. J., Kang, D., & Shim, W. J. (2013). Relationships among the abundances of plastic debris in different size classes on beaches in South Korea. *Marine Pollution Bulletin*, *77*(1–2), 349–354. https://doi.org/10.1016/j.marpolbul.2013.08.013

Li, Y., Zhang, H., & Tang, C. (2020). A review of possible pathways of marine microplastics transport in the ocean. *Anthropocene Coasts*, *3*(1), 6–13. https://doi.org/10.1139/anc-2018-0030

Lotcheris, R. A., Schreyers, L. J., Bui, T. K. L., Thi, K. V. L., Nguyen, H. Q., Vermeulen, B., & van Emmerik, T. H. M. (2024). Plastic does not simply flow into the sea: River transport dynamics affected by tides and floating plants. *Environmental Pollution*, *345*. https://doi.org/10.1016/j.envpol.2024.123524

Maharjan, N., Miyazaki, H., Pati, B. M., Dailey, M. N., Shrestha, S., & Nakamura, T. (2022). Detection of River Plastic Using UAV Sensor Data and Deep Learning. *Remote Sensing*, *14*(13). https://doi.org/10.3390/rs14133049

McFeeters, S. K. (1996). The use of the Normalized Difference Water Index (NDWI) in the delineation of open water features. *International Journal of Remote Sensing*, *17*(7), 1425–1432. https://doi.org/10.1080/01431169608948714

Meijer, L. J. J., van Emmerik, T., van Der Ent, R., Schmidt, C., & Lebreton, L. (2021). More than 1000 rivers account for 80% of global riverine plastic emissions into the ocean. In *Sci. Adv* (Vol. 7). https://www.science.org/doi/10.1126/sciadv.aaz5803

Michel, A. P. M., Morrison, A. E., Preston, V. L., Marx, C. T., Colson, B. C., & White, H. K. (2020). Rapid Identification of Marine Plastic Debris via Spectroscopic Techniques and Machine Learning Classifiers. *Environmental Science and Technology*, *54*(17), 10630–10637. https://doi.org/10.1021/acs.est.0c02099

Moshtaghi, M., Knaeps, E., Sterckx, S., Garaba, S., & Meire, D. (2021). Spectral reflectance of marine macroplastics in the VNIR and SWIR measured in a controlled environment. *Scientific Reports*, *11*(1), 5436. https://doi.org/10.1038/s41598-021-84867-6

Olyaei, M., & Ebtehaj, A. (2024). Uncovering Plastic Litter Spectral Signatures: A Comparative Study of Hyperspectral Band Selection Algorithms. *Remote Sensing*, *16*(1). https://doi.org/10.3390/rs16010172

Pang, K., Kotek, R., & Tonelli, A. (2006). Review of conventional and novel polymerization processes for polyesters. In *Progress in Polymer Science (Oxford)* (Vol. 31, Issue 11, pp. 1009–1037). https://doi.org/10.1016/j.progpolymsci.2006.08.008

Papageorgiou, D., Topouzelis, K., Suaria, G., Aliani, S., & Corradi, P. (2022). Sentinel-2 Detection of Floating Marine Litter Targets with Partial Spectral Unmixing and Spectral Comparison with Other Floating Materials (Plastic Litter Project 2021). *Remote Sensing*, *14*(23). https://doi.org/10.3390/rs14235997

Pedregosa, F., Varoquaux, G., Gramfort, A., Michel, V., Thirion, B., Grisel, O., Blondel, M., Prettenhofer, P., Weiss, R., Dubourg, V., Vanderplas, J., Passos, A., Cournapeau, D., Brucher, M., Perrot, M., & Duchesnay, É. (2011). Scikit-learn: Machine Learning in Python. *The Journal of Machine Learning Research*, *12*, 2825–2830.

Rillig, M. C. (2012). Microplastic in terrestrial ecosystems and the soil? In *Environmental Science and Technology* (Vol. 46, Issue 12, pp. 6453–6454). https://doi.org/10.1021/es302011r

Rouse, J. W., Haas, R. H., Schell, J. A., & Deering, D. W. (1974). Monitoring vegetation systems in the Great Plains with ERTS. *NASA. Goddard Space Flight Center 3d ERTS-1 Symp.*, *1*.

Sakti, A. D., Sembiring, E., Rohayani, P., Fauzan, K. N., Anggraini, T. S., Santoso, C., Patricia, V. A., Ihsan, K. T. N., Ramadan, A. H., Arjasakusuma, S., & Candra, D. S. (2023). Identification of illegally dumped plastic waste in a highly polluted river in Indonesia using Sentinel-2 satellite imagery. *Scientific Reports*, *13*(1). https://doi.org/10.1038/s41598-023-32087-5

SAL Engineering, Eoptis, & Fondazione Bruno Kessler. (2018). *MAIA The multispectral camera: Datasheet*. https://www.spectralcam.com/wp-content/uploads/2020/04/MAIA_S2_Datasheet_Rev_0.3.pdf

Savitzky, A., & Golay, M. J. E. (1964). Smoothing and Differentiation of Data by Simplified Least Squares Procedures. *Anal. Chem.*, *36*(8), 1627–1639. https://doi.org/10.1021/ac60214a047

Schmidt, T., Kuester, T., Smith, T., & Bochow, M. (2023). Potential of Optical Spaceborne Sensors for the Differentiation of Plastics in the Environment. *Remote Sensing*, *15*(8). https://doi.org/10.3390/rs15082020

Schreyers, L. J., Hauk, R., Wallerstein, N., Teuling, A. J., Uijlenhoet, R., & Van Der Ploeg, M. (2025). *Flood type drives river-scale plastic deposition [Preprint]*. https://doi.org/10.31223/X57B01

Schreyers, L., Van Emmerik, T., Biermann, L., & Van Der Ploeg, M. (2022). Direct and Indirect River Plastic Detection from Space. *International Geoscience and Remote Sensing Symposium (IGARSS)*, *2022-July*, 5539–5542. https://doi.org/10.1109/IGARSS46834.2022.9883379

Schreyers, L., van Emmerik, T., Nguyen, T. L., Castrop, E., Phung, N. A., Kieu-Le, T. C., Strady, E., Biermann, L., & van der Ploeg, M. (2021). Plastic Plants: The Role of Water Hyacinths in Plastic Transport in Tropical Rivers. *Frontiers in Environmental Science*, *9*. https://doi.org/10.3389/fenvs.2021.686334

Seelig, H. -D., Hoehn, A., Stodieck, L. S., Klaus, D. M., Adams III, W. W., & Emery, W. J. (2008). The assessment of leaf water content using leaf reflectance ratios in the visible, near-, and short-wave-infrared. *International Journal of Remote Sensing*, *29*(13), 3701–3713. https://doi.org/10.1080/01431160701772500

Strungaru, S. A., Jijie, R., Nicoara, M., Plavan, G., & Faggio, C. (2019). Micro- (nano) plastics in freshwater ecosystems: Abundance, toxicological impact and quantification methodology. In *TrAC - Trends in Analytical Chemistry* (Vol. 110, pp. 116–128). Elsevier B.V. https://doi.org/10.1016/j.trac.2018.10.025

Tasseron, P., van Emmerik, T., Peller, J., Schreyers, L., & Biermann, L. (2021). Advancing floating macroplastic detection from space using experimental hyperspectral imagery. *Remote Sensing*, *13*(12). https://doi.org/10.3390/rs13122335

Themistocleous, K., Papoutsa, C., Michaelides, S., & Hadjimitsis, D. (2020). Investigating detection of floating plastic litter from space using sentinel-2 imagery. *Remote Sensing*, *12*(16). https://doi.org/10.3390/RS12162648

Topouzelis, K., Papageorgiou, D., Karagaitanakis, A., Papakonstantinou, A., & Ballesteros, M. A. (2020). Remote sensing of sea surface artificial floating plastic targets with Sentinel-2 and unmanned aerial systems (plastic litter project 2019). *Remote Sensing*, *12*(12). https://doi.org/10.3390/rs12122013

Tramoy, R., Gasperi, J., Colasse, L., & Tassin, B. (2020). Transfer dynamic of macroplastics in estuaries — New insights from the Seine estuary: Part 1. Long term dynamic based on date-prints on stranded debris. *Marine Pollution Bulletin*, *152*. https://doi.org/10.1016/j.marpolbul.2020.110894

Tu, Y. H., Johansen, K., Aragon, B., El Hajj, M. M., & McCabe, M. F. (2022). The radiometric accuracy of the 8-band multi-spectral surface reflectance from the planet SuperDove constellation. *International Journal of Applied Earth Observation and Geoinformation*, *114*. https://doi.org/10.1016/j.jag.2022.103035

van Emmerik, T., Frings, R. M., Schreyers, L. J., Hauk, R., de Lange, S. I., & Mellink, Y. A. M. (2023b). River plastic transport and deposition amplified by extreme flood. *Nature Water*, *1*(6), 514–522. https://doi.org/10.1038/s44221-023-00092-7

van Emmerik, T., Kirschke, S., Schreyers, L. J., Nath, S., Schmidt, C., & Wendt-Potthoff, K. (2023a). Estimating plastic pollution in rivers through harmonized monitoring strategies. *Marine Pollution Bulletin*, *196*. https://doi.org/10.1016/j.marpolbul.2023.115503

van Emmerik, T., Mellink, Y., Hauk, R., Waldschläger, K., & Schreyers, L. (2022). Rivers as Plastic Reservoirs. *Frontiers in Water*, *3*. https://doi.org/10.3389/frwa.2021.786936

Van Emmerik, T., Roebroek, C., De Winter, W., Vriend, P., Boonstra, M., & Hougee, M. (2020). Riverbank macrolitter in the Dutch Rhine-Meuse delta. *Environmental Research Letters*, *15*(10). https://doi.org/10.1088/1748-9326/abb2c6

van Emmerik, T., & Schwarz, A. (2020). Plastic debris in rivers. *Wiley Interdisciplinary Reviews: Water*, *7*(1), 1–24. https://doi.org/10.1002/wat2.1398

Veettil, B. K., Hong Quan, N., Hauser, L. T., Doan Van, D., & Quang, N. X. (2022). Coastal and marine plastic litter monitoring using remote sensing: A review. In *Estuarine, Coastal and Shelf Science* (Vol. 279). Academic Press. https://doi.org/10.1016/j.ecss.2022.108160

Villa, P., Mousivand, A., & Bresciani, M. (2014). Aquatic vegetation indices assessment through radiative transfer modeling and linear mixture simulation. *International Journal of Applied Earth Observation and Geoinformation*, *30*, 113–127. https://doi.org/10.1016/j.jag.2014.01.017

Vriend, P., Roebroek, C. T. J., & van Emmerik, T. (2020). Same but Different: A Framework to Design and Compare Riverbank Plastic Monitoring Strategies. *Frontiers in Water*, *2*. https://doi.org/10.3389/frwa.2020.563791

Yang, D., Chen, J., Zhou, Y., Chen, X., Chen, X., & Cao, X. (2017). Mapping plastic greenhouse with medium spatial resolution satellite data: Development of a new spectral index. *ISPRS Journal of Photogrammetry and Remote Sensing*, *128*, 47–60. https://doi.org/10.1016/j.isprsjprs.2017.03.002

Yee, M. S. L., Hii, L. W., Looi, C. K., Lim, W. M., Wong, S. F., Kok, Y. Y., Tan, B. K., Wong, C. Y., & Leong, C. O. (2021). Impact of microplastics and nanoplastics on human health. In *Nanomaterials* (Vol. 11, Issue 2, pp. 1–23). MDPI AG. https://doi.org/10.3390/nano11020496

Appendix I: Satellite characteristics

Table 3 *Characteristics of each satellite type studied (Copernicus EU & European Space Agency, n.d.; Planet Labs Inc., 2025; EnMAP, 2022).*

	Sentinel-2	**PlanetScope SuperDove**	**EnMAP**
Spectral bands and equivalent wavelengths	1. Coastal aerosol 442.7 nm 2. Blue 492.7 nm 3. Green 559.8 nm 4. Red 664.6 nm 5. Red edge 1 704.1 nm 6. Red edge 2 740.5 nm 7. Red edge 3 782.8 nm 8. NIR 1 832.8 nm 8a. NIR 2 864.7 nm 9. Water vapour 945.1 nm 10. SWIR – Cirrus 1373.5 nm 11. SWIR 1 1613.7 nm 12. SWIR 2 2202.4 nm	1. Coastal Blue 443 nm 2. Blue 490 nm 3. Green I 531 nm 4. Green 565 nm 5. Yellow 610 nm 6. Red 665 nm 7. Red Edge 705 nm 8. NIR 865 nm	- 228 spectral bands - Spectral range: 420 nm - 2450 nm - Intervals of 6.5 nm and 10 nm for the VNIR and SWIR bands
Spatial resolution	Band 2, 3, 4, 8: 10 m Band 5, 6, 7, 8a, 11, 12: 20 m Band 1, 9, 10: 60 m	3 m	30 m
Revisit time	~ 5 days	~ 1 day	Based on observation requests

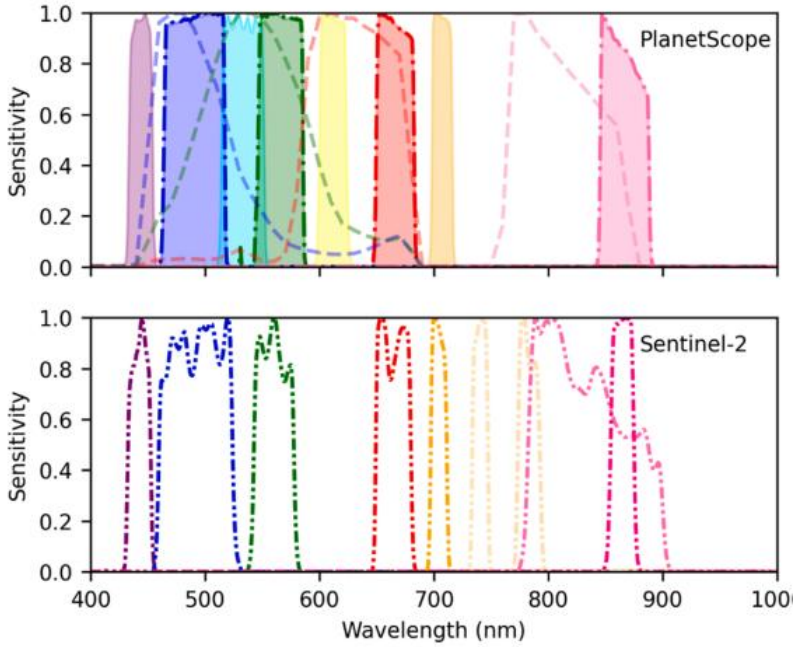

PlanetScope SuperDove bands	**Interoperable with Sentinel-2**
Band 1	Band 1
Band 2	Band 2
Band 3	No
Band 4	Band 3
Band 5	No
Band 6	Band 4
Band 7	Band 5
Band 8	Band 8a

Figure 7 *The spectral response functions of different generations of PlanetScope satellites and of the first nine bands of Sentinel-2. Out of the PlanetScope satellites, the SuperDove is relevant for this thesis. It can be seen that certain bands of PlanetScope and Sentinel-2 are interoperable. (Tu et al., 2022).*

Appendix II: Land covers and HSR measurements

Table 4 *Land covers in the study area and information on the HSR measurements. The images of the polyester target with a grass background and the multiple layers of polyester are the same, because the multiple layers visually looked the same. However, the HSR did not measure the same values.*

Land covers measured by the HSR	**Amount of measurements**	**Estimated diameter of FOV**	**Image**
Polyester target with a grass background	5	60 cm	
Multiple layers of polyester	3	23 cm	
PET bottle target with a grass background*	3	23 cm	
PET bottle target with a soil background	3	23 cm	
Shrubs	5	30 cm	
Grass	10	60 cm	
Riparian vegetation	5	23 cm	
Rock	5	60 cm	
Water	5	51 cm	
Sand	11	60 cm	
Soil	2 (total = 12) 5 5	23 cm 30 cm 60 cm	

Appendix III: Field measurement devices

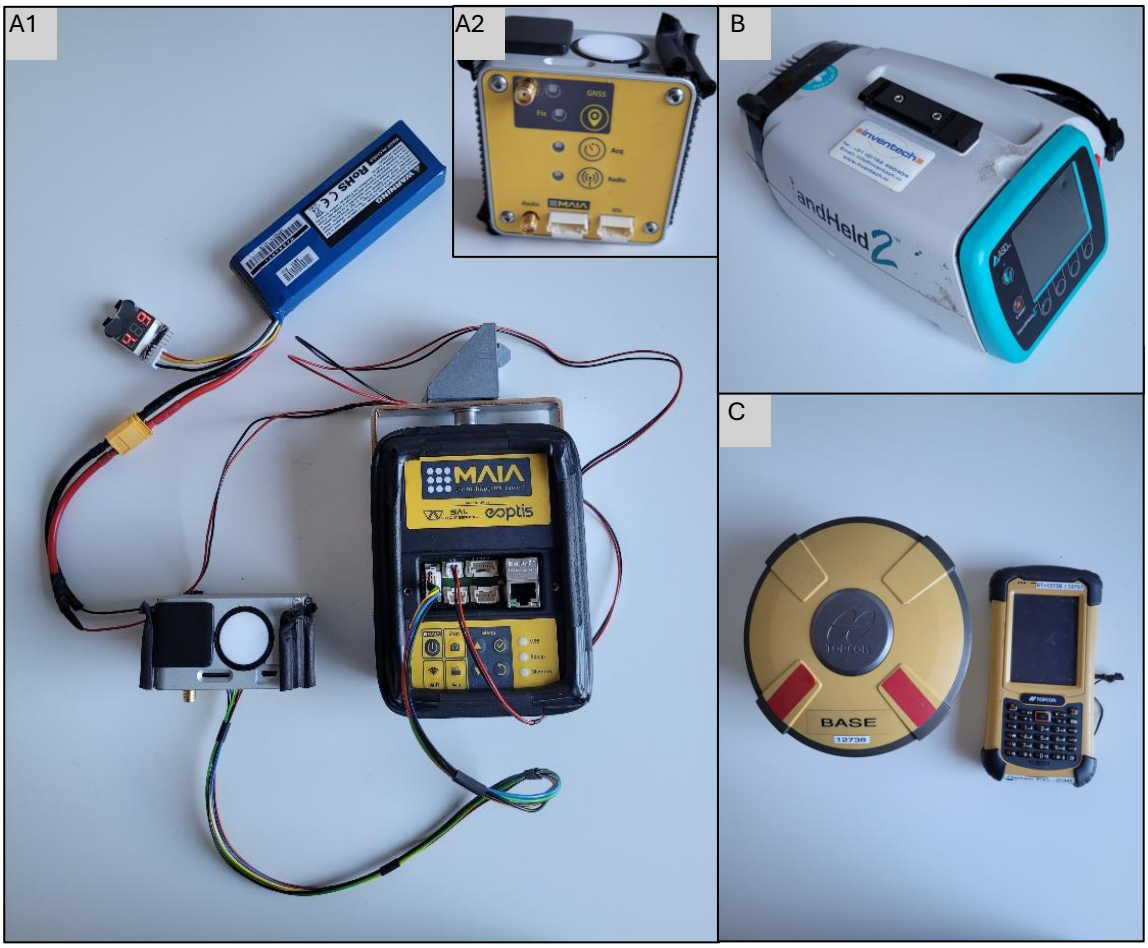

Figure 8 A1) *The MAIA S2 camera attached to a battery and the Incident Light Sensor (ILS).* ***A2)*** *The ILS.* ***B)*** *The ASD Fieldspec Handheld 2 Spectroradiometer.* ***C)*** *The Topcon HiPer V GNSS receiver.*

Appendix IV: Spectral Indices

Table 5 *The spectral indices used in this study.*

Index	Formula	Description	Source
Normalised Difference Vegetation Index (NDVI)	$NDVI = \frac{(NIR - RED)}{(NIR + RED)}$	Useful for differentiation between river water and vegetation.	(Rouse et al., 1974)
Normalised Difference Aquatic Vegetation Index (NDAVI)	$NDAVI = \frac{(NIR - BLUE)}{(NIR + BLUE)}$	Useful for differentiation between river water and vegetation.	(Villa et al., 2014)
Normalised Difference Water Index (NDWI)	$NDWI = \frac{(GREEN - NIR)}{(GREEN + NIR)}$	Useful for differentiation between river water and vegetation.	(McFeeters, 1996)
Floating Debris Index (FDI)	$FDI = B08 - B06 - (B11 - B06) * \frac{10(\lambda_{B08} - \lambda_{B04})}{(\lambda_{B11} - \lambda_{B04})}$	To detect floating pollution in the ocean. By using this index, it was shown for the first time that floating macroplastics are detectable in Sentinel-2 imagery.	(Biermann et al., 2020)
Plastics Index (PI)	$PI = \frac{NIR}{(NIR + RED)}$	PI was developed for Sentinel-2 data and showed to be effective for detecting floating plastic on the ocean.	(Themistocleous et al., 2020)
Adjusted Plastic Index (API)	$NDBI = \frac{(SWIR - NIR)}{(SWIR + NIR)}$ IF NDVI > 0 $PI_1 = PI - NDVI$ $ELSE$ $PI_1 = PI$ IF NDBI > 0 $PI_2 = PI_1 - NDBI$ $ELSE$ $PI_1 = PI_2$	PI adjusted for river areas. API is not only based on PI, but also on NDVI and the Normalised Difference Built-up Index (NDBI).	(Sakti et al., 2023)
Plastic Greenhouse Index (PGI)	$IF\ NDVI > 0.73 \quad PGI = 0$ $IF\ NDBI > 0.005\ PGI = 0$ $ELSE$ $PGI = 100 * \frac{BLUE * (NIR - RED)}{1 - mean(BLUE + GREEN + NIR)}$	Developed to map plastic greenhouses over large areas. There are similarities between the plastic targets and the plastic greenhouses (PGs). Both the PET target and the PGs were transparent, were lying over a	(Yang et al., 2017)

		vegetation cover, and collected condense.	
Plastic Patch Index (PPI)	$PPI = \frac{(B08a - B09)}{(B08a + B09)}$	The formula is given in terms of Sentinel-2 bands.	(Breukel, 2025)
SI-13	$SI13 = \frac{(B03 - B01)}{(B03 + B01)}$	Newly developed spectral index. The formula is given in terms of Sentinel-2 bands, but can be applied to all other sensors used in this research.	-
SI-23	$SI23 = \frac{(B03 - B02)}{(B03 + B02)}$	Newly developed spectral index. The formula is given in terms of Sentinel-2 bands, but can be applied to all other sensors used in this research.	-

Appendix V: Enlarged versions of the Sentinel-2 spectra

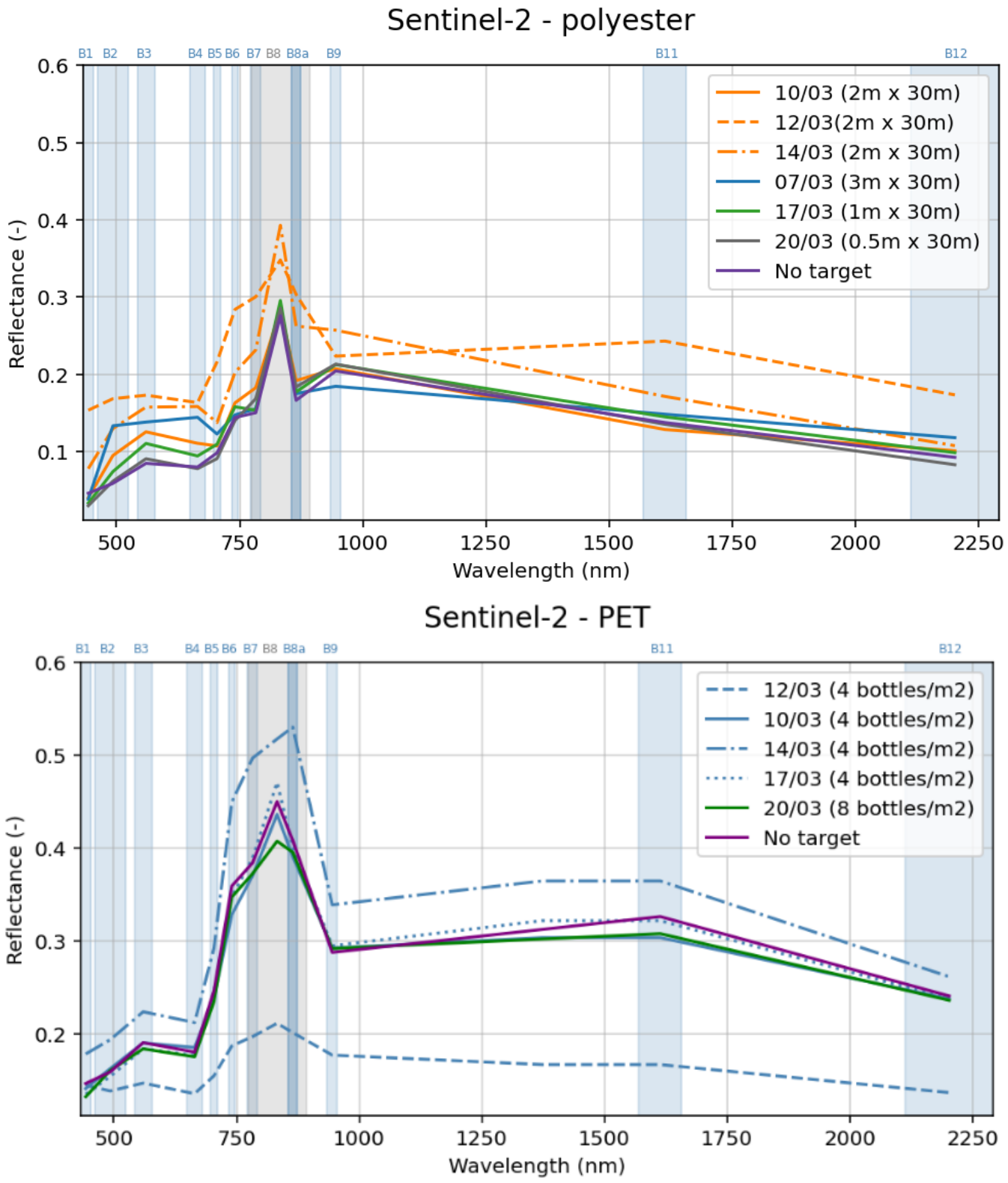

Figure 9 *Enlarged versions of the Sentinel-2 reflectance spectra of different polyester and PET coverages.*

Appendix VI: Spectral index maps

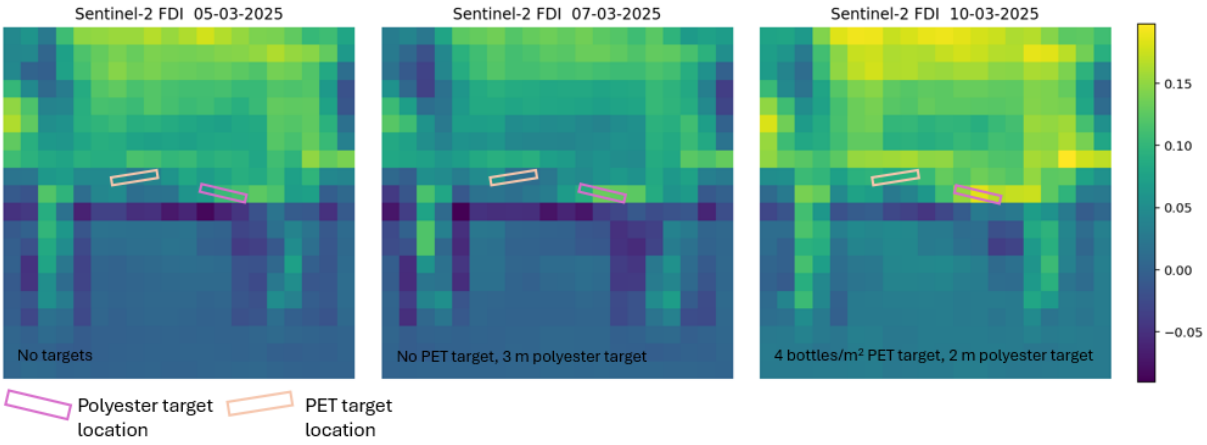

Figure 10 *FDI map. The FDI values of the riverbank land covers are not very stable between the images. The index was designed to distinguish floating debris from water pixels. The FDI values of water pixels are indeed more stable. The polyester target shows relatively high FDI values compared to its surroundings, but the target is not clearly distinguishable from all other land covers. High values also occur at other locations within the study area, e.g. at the top of the image. The PET target is not distinguishable.*

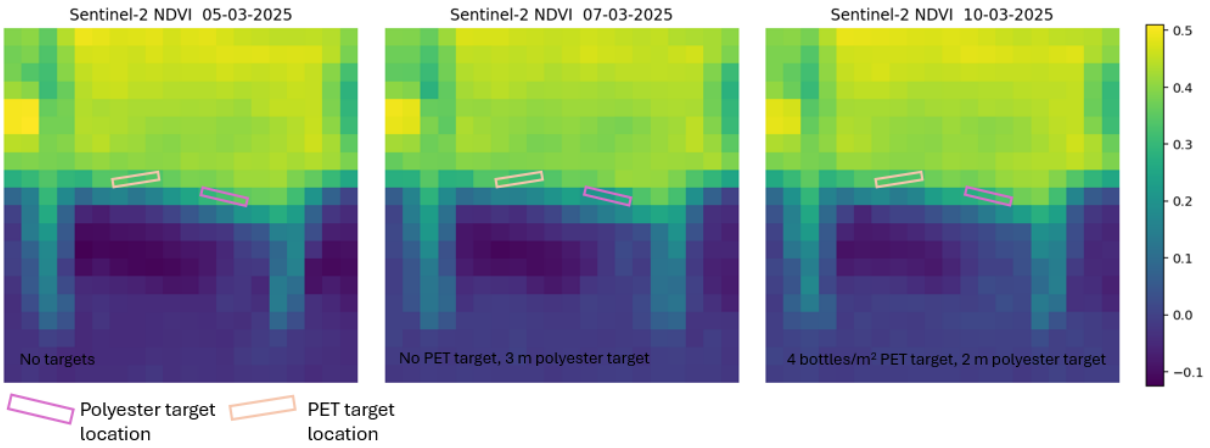

Figure 11 *NDVI map. NDVI mainly distinguishes between vegetation and water and shows intermediate values around the border of land and water. The plastic targets are not distinguishable.*

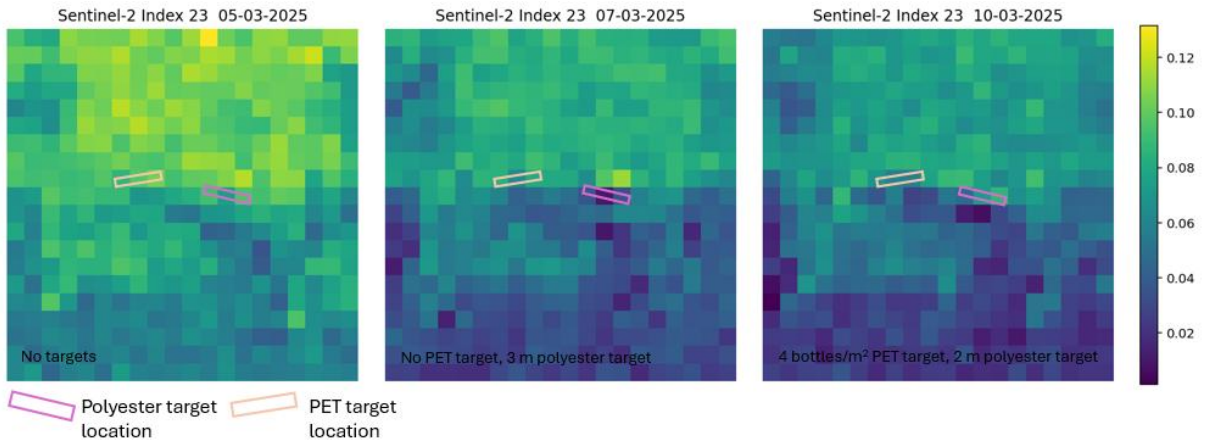

Figure 12 *SI-23 map. The right polyester pixel has the highest value within the image of the 3 m polyester target, but this does not hold anymore for smaller polyester targets. The PET target is not distinguishable.*

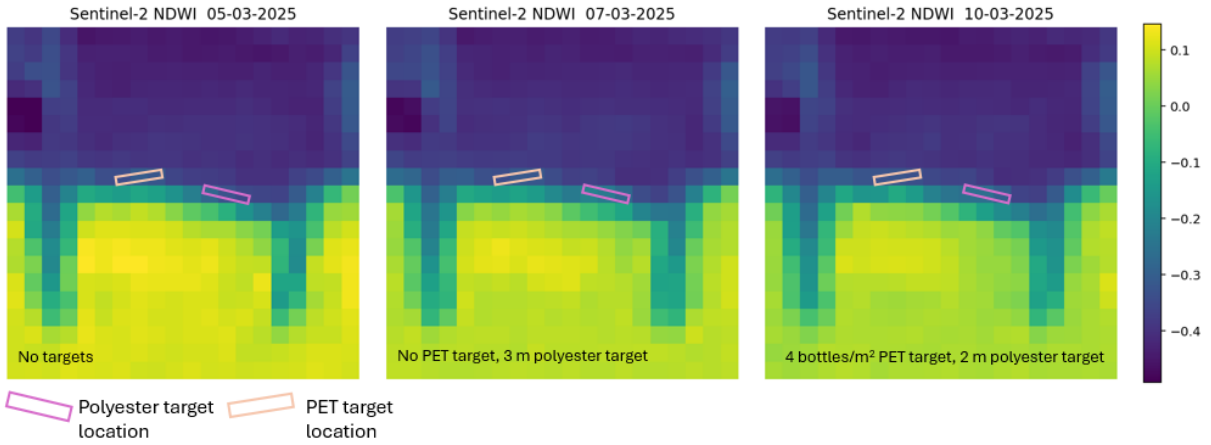

Figure 13 *NDWI map. NDWI roughly shows the reverse effect of NDVI. There are high values at water pixels and low values at vegetation pixels. The plastic targets are not distinguishable.*

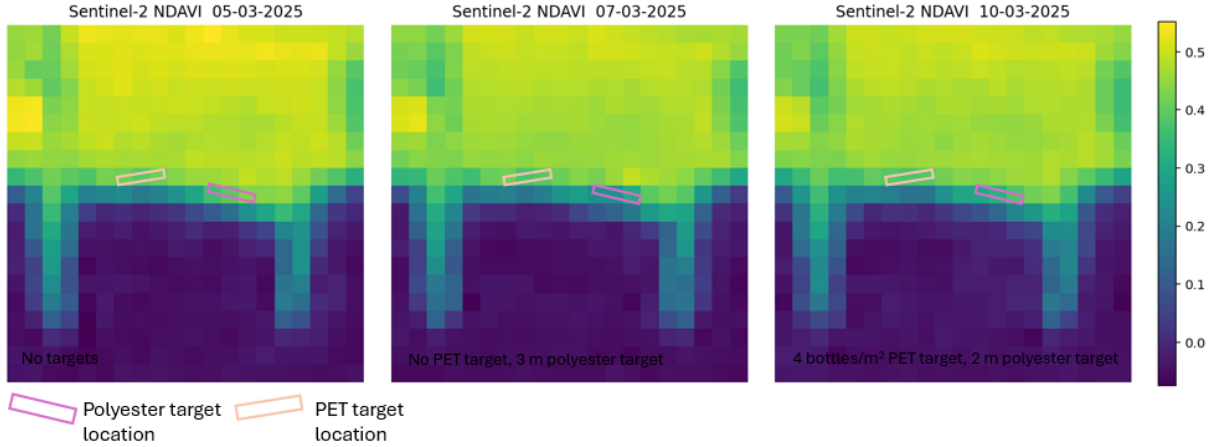

Figure 14 *NDAVI map. No clear signals are coming from the targets. The right polyester pixel has a slightly higher value compared to its surroundings. This is, however, not a strong deviation from the other values within the image. The effect is gone in images of smaller polyester targets.*

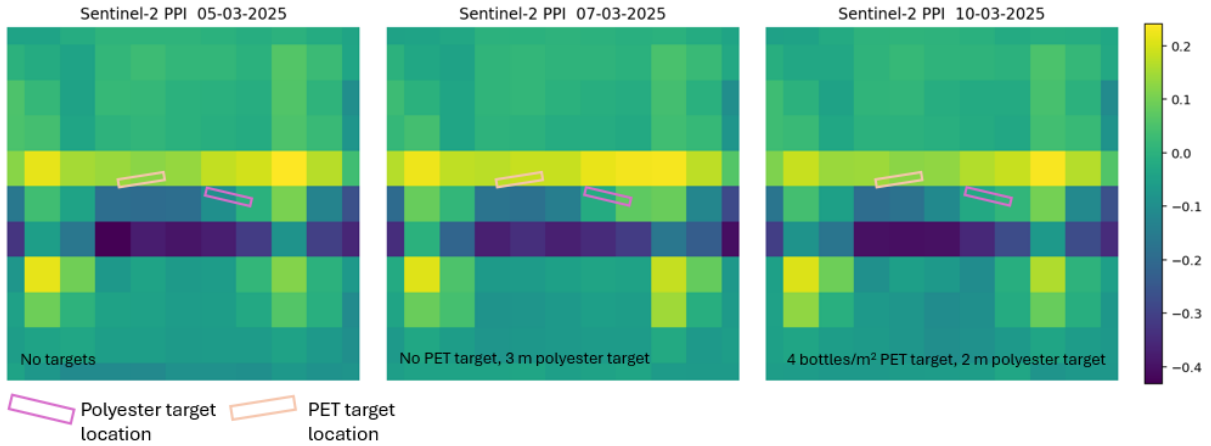

Figure 15 *PPI map. PPI is not based on bands with a 10m resolution, meaning it can only predict at 20 m resolution. The pixels that belong to the 3 m polyester target are relatively bright, but are not easily distinguishable from all other pixels within the image. There is no clear signal of the PET target.*

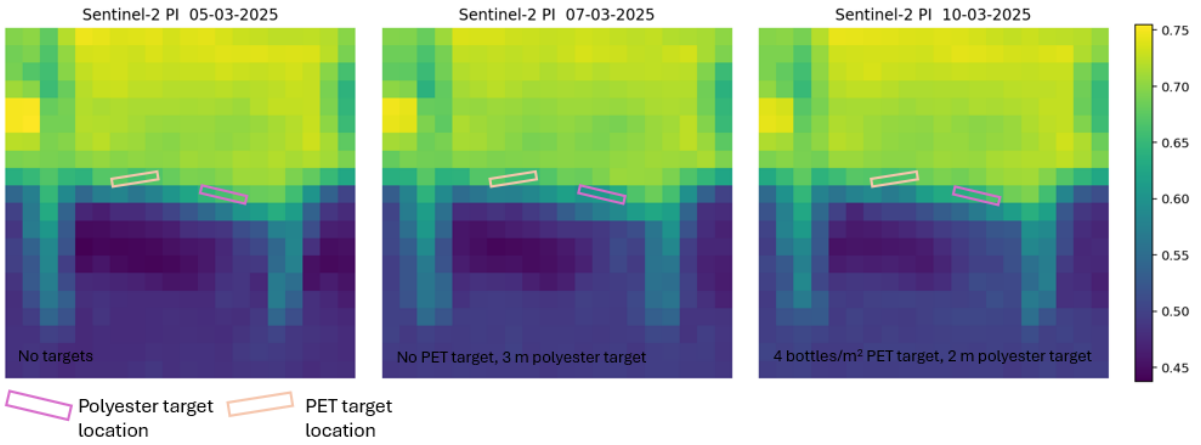

Figure 16 *PI map. No plastic target is distinguishable.*

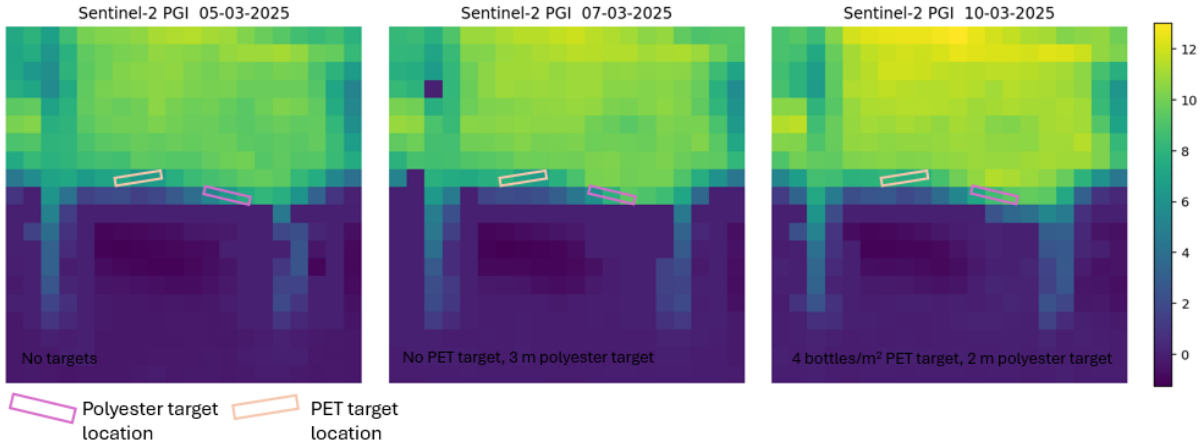

Figure 17 *PGI map. No plastic target is distinguishable.*

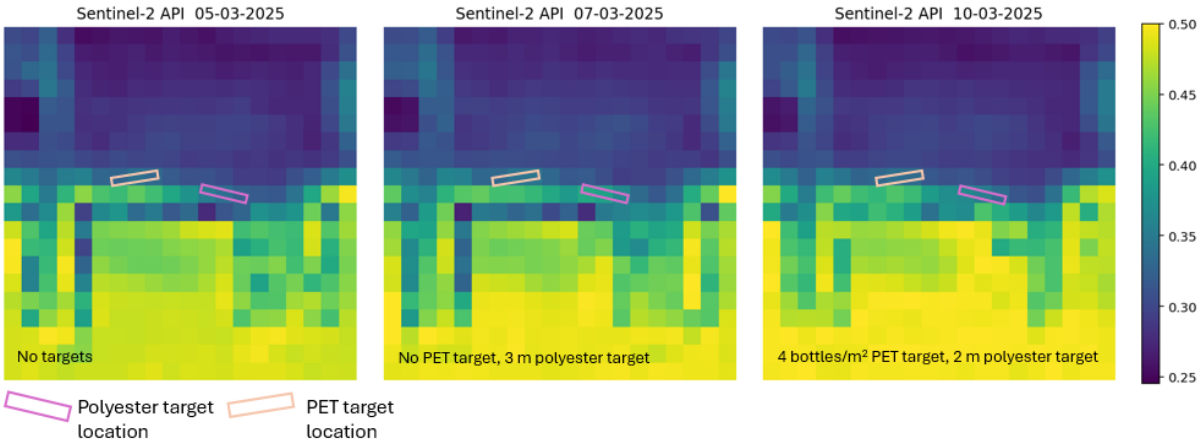

Figure 18 *API map. There are somewhat higher API values at the polyester target pixels compared to the scenario without targets on 5 March. However, the plastic pixel values are in the same range as a part of the other values and thus cannot be clearly distinguished from the environment.*

Appendix VII: Naive Bayes classification

Table 6 *Results of method 2 with Naive Bayes trained on default priors.*

Polyester target	Pixel	Prediction class	Pixel plastic coverage 10m band
3 m x 30 m	Left	Sand	26.7%
0.5 m x 30 m	All	Vegetation	4.3-5.3%
3 m x 30 m **2 m x 30 m** **1 m x 30 m**	Middle, right All All	Polyester	8.5-24.6%, 29.6%

Table 7 *Results of method 2 with Naive Bayes trained on equal priors.*

Polyester target	Pixel	Prediction class	Pixel plastic coverage 10m band
3 m x 30 m	Left	Sand	26.7%
0.5 m x 30 m	Right	Vegetation	4.3%
3 m x 30 m **2 m x 30 m** **1 m x 30 m** **0.5 m x 30 m**	Middle, right All All Left, middle	Polyester	5.1-24.6%, 29.6%

Table 8 *Accuracy metrics of method 3 with Naive Bayes trained on default priors.*

Target	Precision	Recall	F1-score	Overall accuracy
3 m x 30 m	0.25	0.33	0.29	0.97
2 m x 30 m	0.43	1.00	0.60	0.97
1 m x 30 m	0.33	1.00	0.50	0.97
0.5 m x 30 m	0.00	0.00	0.00	0.95

Table 9 *Accuracy metrics of method 3 with Naive Bayes trained on equal priors.*

Target	Precision	Recall	F1-score	Overall accuracy
3 m x 30 m	0.08	0.33	0.13	0.94
2 m x 30 m	0.20	1.00	0.33	0.96
1 m x 30 m	0.20	1.00	0.33	0.95
0.5 m x 30 m	0.18	0.67	0.29	0.95

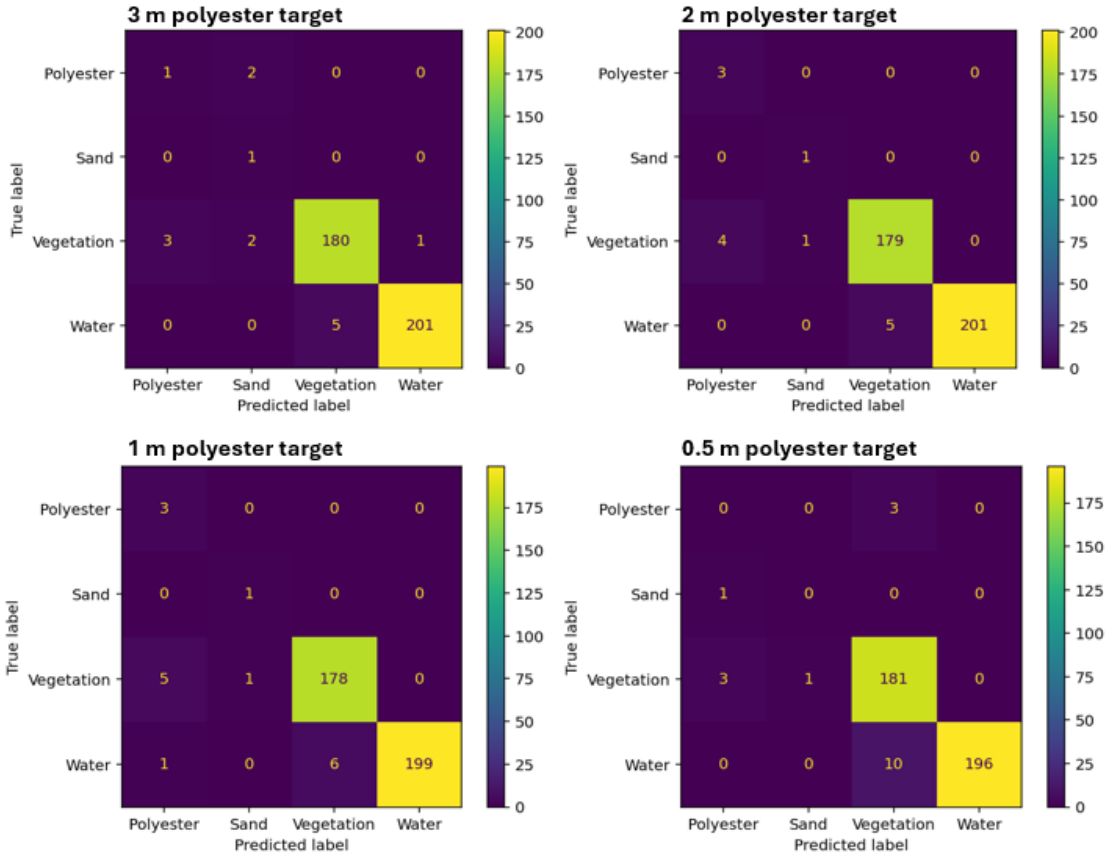

Figure 19 *Confusion matrices of method 3 with Naive Bayes trained on default priors.*

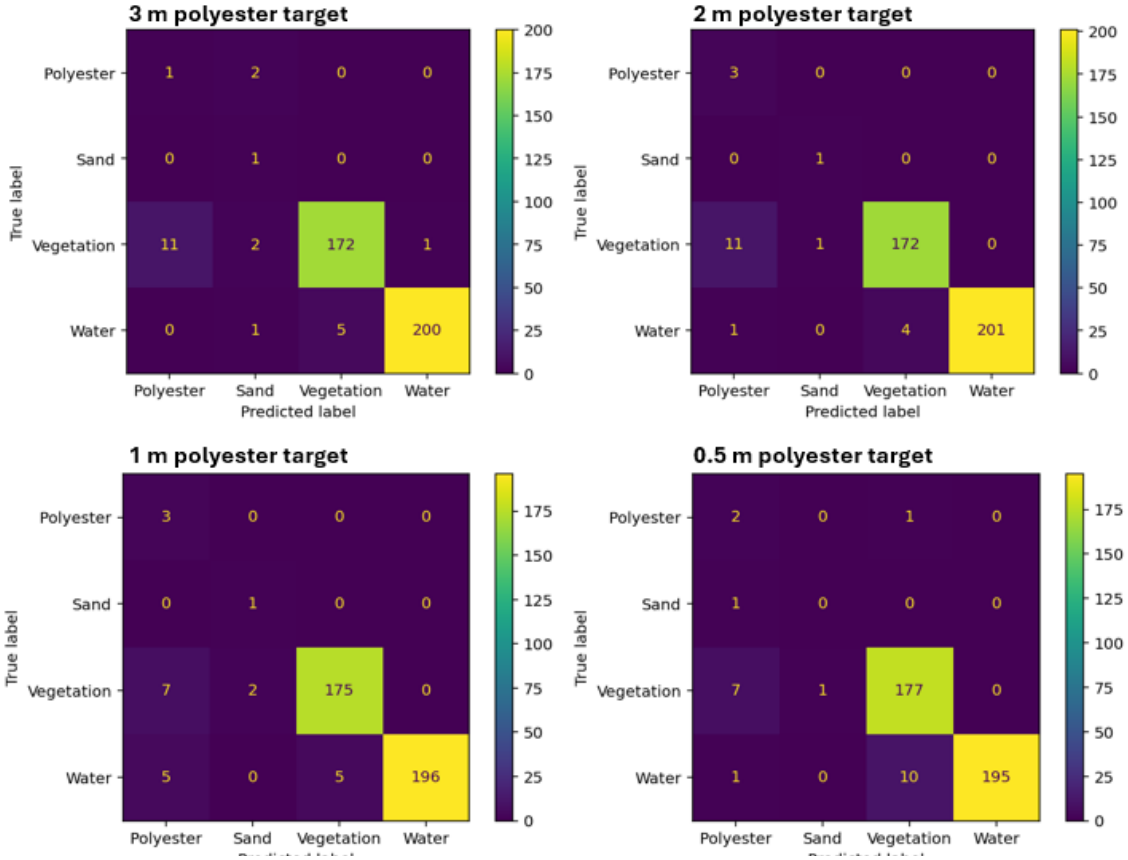

Figure 20 *Confusion matrices of method 3 with Naive Bayes trained on equal priors.*

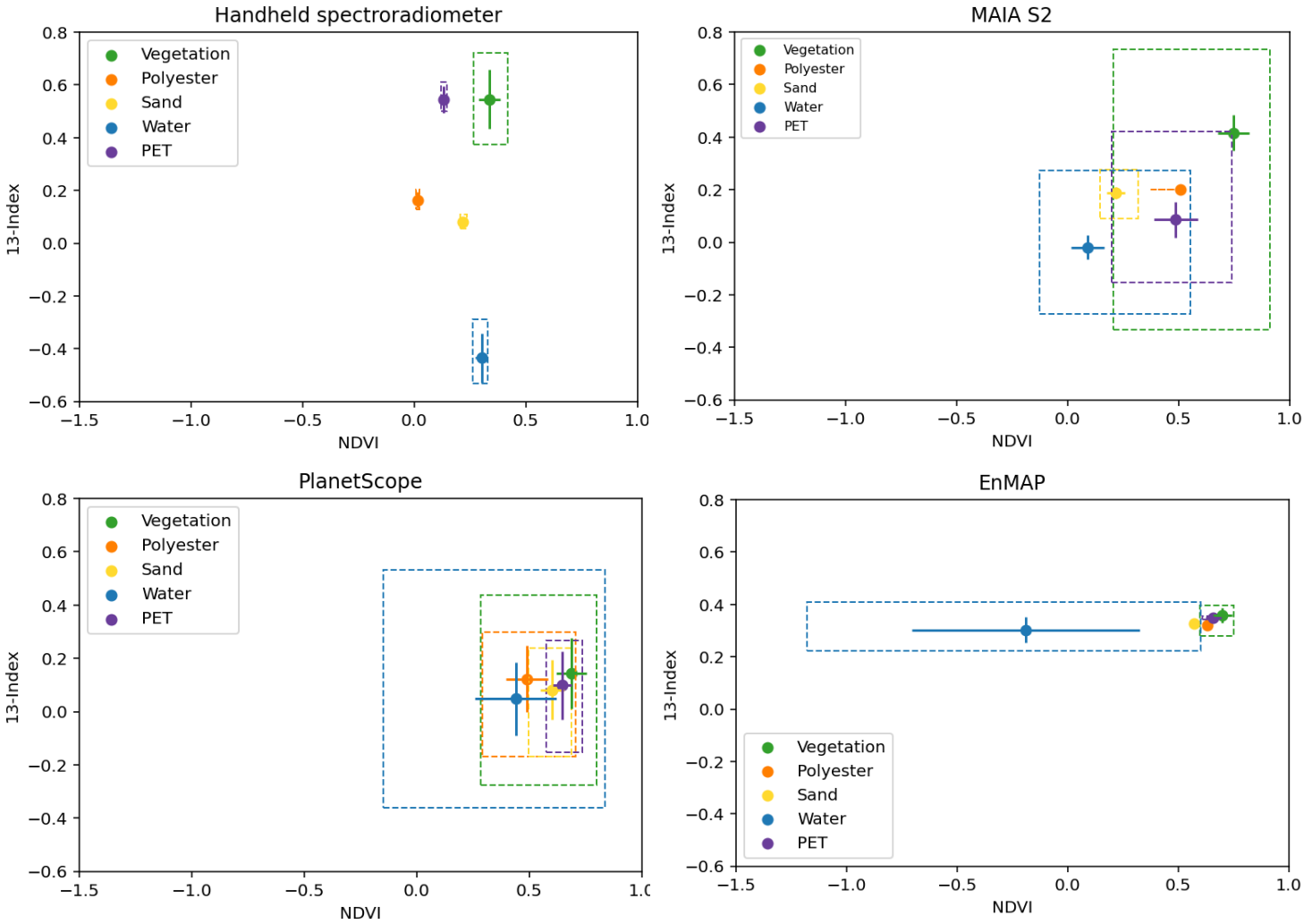

Figure 21 *SI-13 and NDVI clustering for other sensors than Sentinel-2. In comparison to the other sensors, the HSR could distinguish between each class. Therefore, for the HSR all land covers in the study area are shown instead of the land covers used for plastic detection in Sentinel-2 imagery.*

Appendix VIII: Use of Generative AI statement

Grammarly

Grammarly was used as a grammar and spelling checker for the final thesis report. The tool was used right before submitting the thesis report. For every correction, it was first checked whether the correction was appropriate. Using Grammarly has led to the improvement of spelling and grammar in the thesis report.

ChatGPT

ChatGPT was utilised in several ways, as listed below. The purpose of the usage and how it affected the research are described.

Coding support

ChatGPT was mainly used as a coding assistant. It was used to find and solve coding errors, to find what libraries, functions, and prompts are useful for specific actions, and to make code more efficient. By using the AI tool in these ways, the coding process became more efficient, it made the code easier to understand, and it supported the learning process of the student by showing how to improve the code. The output of ChatGPT was first studied before using it for coding. The student made sure to understand the code first to maintain the quality of the code.

Explaining concepts

ChatGPT was used to explain how certain concepts worked related to statistics and remote sensing pre-processing and analysis. The purpose was to get a first impression of how these concepts work. However, the output was reflected on critically by assessing whether the output made any sense to start with. In addition, other sources were used to verify the output of ChatGPT. Information provided by ChatGPT was only used when the student was sure that it was correct.

ArcGIS Pro support

ChatGPT was used as support for using the software of ArcGIS Pro. When the student did not know how to carry out certain actions in the software, they asked ChatGPT. Sometimes, ArcGIS Pro did not support the actions directly, and suggestions were made by ChatGPT to do it in a different way. This method was only used if it made sense to the student. The use of ChatGPT supported the learning process of the student (by giving insight into how ArcGIS Pro was functioning) and made it more efficient. There was no direct impact on the research outcomes, as it was easily assessed whether the suggestions made by ChatGPT were helpful or not.